U.S. Department of Transportation
Federal Aviation Administration

FINAL PROJECT REPORT

Form Approved:
O.M.B. No. 2120-0559
9/30/2013

PART I - PROJECT IDENTIFICATION INFORMATION

1. Institution and Address	2. FAA Program	3. FAA Award Number
Georgia Tech Research Corporation	AJFE	13-C-AJFE-GIT-057
926 Dalney Street NW, Atlanta, Georgia 30332-0415	4. Award Period From 2/5/2020 To 2/29/2024	5. Cumulative Award Amount $890,000

6. Project Title
Over-Wing Engine Placement Evaluation

PART II - SUMMARY OF COMPLETED PROJECT (For Public Use)

The over-wing nacelle (OWN) aircraft concept has promising environmental benefits due to the engine noise shielding by the wings. However, if not optimized, this engine placement may cause penalties in fuel burn due to adverse aerodynamic interactions between the wing and propulsor. In this work, the team aims to develop a multi-disciplinary optimization method for OWN aircraft. The goal is to provide FAA stakeholders with evidence to gauge the intrinsic aero-propulsive (dis)advantages of OWN vs. underwing nacelle (UWN) designs. We initially and deliberately assumed the same engine and aircraft size while optimizing both configurations. We found a 4% higher fuel flow at cruise for the OWN. We also linked the aero-propulsion analyses to mission flight path optimization. This optimized OWN configuration has approximately 7% higher fuel burn than a similarly optimized UWN over a reference mission. We also conducted a physics study of low speed/high lift configurations of OWN and UWN. We found that the OWN placement provided significant improvements in aerodynamic characteristics, but only a relatively modest improvement in takeoff field length. We then repeated the aerodynamic optimization for an aft mounted OWN configuration. The resulting design had a 5% higher fuel burn at cruise compared to the UWN. We then designed a new engine cycle to reflect recent technology levels, and the larger bypass engine was used in both OWN and UWN optimizations. We found that the OWN still had substantially higher fuel burn than the UWN.

PART III - TECHNICAL INFORMATION (For Program Management Uses)

1. ITEM (Check appropriate blocks)	NONE	ATTACHED	PREVIOUSLY FURNISHED	TO BE FURNISHED SEPARATELY TO PROGRAM	
				Check (X)	Approx. Date
a. Abstracts of Theses	X				
b. Publication Citations		X			
c. Data on Scientific Collaborators		X			
d. Information on Inventions	X				
e. Technical Description of Project and Results		X			
f. Other (specify)					

2. Principal Investigator/Project Director Name (Typed)	3. Principal Investigator / Project Director Signature	4. Date
Dimitri N. Mavris	DocuSigned by: Dimitri Mavris 5809B757C58D414...	3/11/2024 | 2:55 PM EDT

FAA Form 9550-5 (03-03) Supersedes Previous Edition

Project 050 Over-Wing Engine Placement Evaluation

Final Report

Georgia Institute of Technology

Project Lead Investigators

Principal Investigator:
Professor Dimitri N. Mavris
Director, Aerospace Systems Design Laboratory
School of Aerospace Engineering
Georgia Institute of Technology
Phone: (404) 894-1557
Fax: (404) 894-6596
Email: dimitri.mavris@ae.gatech.edu

Co-Principal Investigator:
Dr. Chung Lee
Research Engineer
Aerospace Systems Design Laboratory
School of Aerospace Engineering
Georgia Institute of Technology
Phone (c/o): (404) 894-0197
Fax: (404) 894-6596
Email (c/o): jimmy.tai@ae.gatech.edu

University Participants

Georgia Institute of Technology

- P.I.: Dr. Dimitri Mavris and Co-P.I. Dr. Chung Lee
- FAA Award Number: 13-C-AJFE-GIT-057
- Period of Performance: February 5, 2020 through February 29, 2024
- Tasks relevant for this period:
    1. Creation of single aisle aircraft mission model and a baseline high bypass turbofan propulsion cycle model
    2. Parametric geometry generation
    3. Formulation of MDAO problem
    4. Generation of CFD templates and automation scripts
    5. Stage 1 design: nacelle and wing optimization (forward mounted OWN)
    6. Create ANOPP noise models
    7. Stage 2 design: engine re-design and airframe re-optimization (forward mounted OWN)
    8. Stage 3 design: nacelle and wing optimization (aft mounted OWN)
    9. Trajectory optimization and mission analysis
    10. Takeoff/high lift physics study

Project Funding Level

Georgia Institute of Technology (Georgia Tech) was initially funded at $590,000 for a two-year project. Georgia Tech agreed to a total of $590,000 in matching funds. Georgia Tech was then funded an additional at $300,000 for a one-year project extension. Georgia Tech agreed to a total of $300,000 in matching funds. This total includes salaries for the project director, research engineers, and graduate research assistants, as well as computing, financial, and administrative support, including meeting arrangements. The institute has also agreed to provide tuition remission for the students, paid for by state funds.

Investigation Team

PI: Dimitri Mavris
Co-Investigator: Chung Lee

2020
Propulsion and Systems Lead: Jonathan Gladin
Aerodynamics and CAD Geometry: Srujal Patel
Graduate Students: Salah Tarazi, Kenneth Decker, Stephanie Zhu, Christopher Eggert, Andrew Burrell, Christian Perron, and Jai Ahuja

2021-2022
Aerodynamics and Parametric Geometry: Jai Ahuja, Srujal Patel, and Kenneth Decker
MDAO Methods: Christian Perron
Mission and Systems Integration: Evan Harrison
Graduate Students: Mengzhen Chen, Sam Crawford, Marc Koerschner, Bilal Mufti, James Van der Linden, Anish Vegesna, Andrew Burrell, Savri Gandhi, Richard D'Cruz, and Samuel Moore

2023-2024
Aerodynamics and Parametric Geometry: Jai Ahuja and Srujal Patel
Propulsion Lead: Jai Ahuja
MDAO Methods: Christian Perron
Mission and Systems Integration: Evan Harrison
Graduate Students: Samuel Moore, Richard D'Cruz, Savri Gandhi, Bilal Mufti, and Kavya Navaneetha Krishnan

Project Overview

The over-wing nacelle (OWN) aircraft concept has promising environmental benefits due to the engine noise shielding provided by the wings and the potential to reduce landing gear height and therefore gear noise. However, if not optimized, this engine placement may cause penalties in fuel burn due to aerodynamic interactions between the wing and propulsor. In this work, the team aims to develop an MDAO method for OWN aircraft. This task builds on past efforts by including noise shielding effects and optimizing the airframe geometry to minimize cruise fuel burn, and then optimizing the mission flight profile to minimize trip fuel burn. One major challenge is the computational expense of analyses such as computational fluid dynamics (CFD). Thus, the approach relies on multidisciplinary design analysis and optimization (MDAO) and efficient adaptive sampling techniques to use high-fidelity analyses where they are most needed for system analysis.

The optimization of an OWN aircraft configuration over a mission with noise constraints would enable accurate trade-offs between noise benefits and fuel burn. As a secondary benefit, the MDAO method sought to demonstrate efficient sampling methods for coupled, computationally intensive simulations in system analysis. These methods are useful to the FAA because many current applications require high-fidelity simulations to accurately assess physics phenomena such as noise and emissions. Both the OWN results and the MDAO techniques will enable more physics-informed decisions about the environment.

Work in 2020 focused on preliminary tasks to prepare a software tool chain and workflow for optimization, whereas efforts in 2021 focused on the execution of a full-scale MDAO process using supercomputing resources. Thus, the efforts in 2021 focused on a two-stage design process: nacelle location selection and preliminary shape optimization of the wing and nacelle. In 2022, we completed a second-stage shape optimization. We deliberately assumed the same basic engine cycle and aircraft size while optimizing both over-wing and under-wing configurations. We found a 4% higher fuel flow at cruise for the OWN design. However, this preliminary result did not account for higher bypass ratio engines that are possible due to engine clearance above the wing or for other mission segments such as climb. Higher bypass ratio engines were therefore a major focus of 2023 work.

In 2023, we designed a new engine cycle to reflect recent technology levels, and the larger bypass engine was used in both OWN and UWN optimization. In this effort, we also found that the OWN had substantially higher fuel burn than the UWN. However, this year, we also linked the aero-propulsion analyses to mission flight path (trajectory) optimization rather than simply computing fuel flow at a particular Mach and altitude scenario during cruise. The result is that an optimized OWN has approximately 7% higher fuel burn than a similarly optimized UWN over a reference mission. This prediction is based on

governing force-and-motion equations implemented for this effort to facilitate accounting for the intercoupled aero-propulsive effects influential in an OWN design and obtained by an optimal-control trajectory optimization with identical constraints between the two configurations. The researchers feel the results do not provide evidence that the OWN configuration considered here would be more fuel-efficient than its UWN counterpart.

2023 work differs from previous years by emphasizing two subsidiary goals in addition to the comparison of optimized OWN and UWN vehicles. First, we mentioned earlier that a trajectory optimization was conducted in each case to yield not only cruise fuel flow rate but also fuel burn over an entire mission. We used NASA's Dymos optimal controls software and integrated coupled CFD-propulsion surrogates to optimize trajectories to minimize fuel burn. This development allowed a mission-level comparison of fuel burn. Finally, at request of FAA stakeholders, we also conducted a physics study of low speed/high lift configurations of OWN and UWN. The placement of the OWN nacelle allows the jet exhaust plume to blow over the wing, potentially increasing circulation and improving lift (and drag) characteristics. We did not optimize the geometries for takeoff, but simply used the 2022 final geometries that were optimized for cruise and analyzed high lift and takeoff characteristics. We found that even without optimizing for takeoff, the OWN placement provided significant improvements in aerodynamic characteristics. However, when we optimized takeoff trajectories using the OWN and UWN high lift aerodynamic polars, we found that the OWN had a relatively modest improvement in takeoff field length, using methods as in an example code. Our current view is that the OWN vs. UWN takeoff performance may be within the uncertainty of other physics assumptions that we had to make due to the small scope of our study.

Finally, in the last two months of this project's period of performance, we repeated a similar exercise as we did in 2022, but for an aft mounted OWN configuration. Although the baseline aft-mounted design showed substantially lower fuel burn compared to the baseline forward mounted OWN configuration, which initially motivated study into this location, the gains from optimization were much smaller and as such, the resulting design had a 5% higher fuel burn at cruise compared to the UWN.

We emphasized two major themes in research methodology: (a) posing a more controlled comparison of OWN vs. UWN aircraft and (b) carefully accounting for numerical uncertainty. These are repeated here for emphasis.

A more controlled comparison of OWN and UWN aircraft is needed
Physics code uncertainty dominated the MDAO and research strategies. There can be significant discrepancies between un-calibrated CFD predictions and the flight performance of actual vehicles. Therefore, in the absence of validation data, it would be uninformative or misleading to compare the CFD-based performance of an optimized OWN with that of actual UWN vehicles. In addition to the physics discrepancy, there is an inconsistency in the MDAO problem for an OWN study with a two-year scope compared with the UWN configuration, which has been refined by the aircraft industry for around 70 years.

It is not practical for the present OWN study to include more design physics such as flight mechanics, static and dynamic structural constraints, nacelle geometry constraints due to acoustical liners and de-icing components, or pylon aero-thermo-structural mechanics. However, this can result in OWN performance that is overly optimistic due to an under-constrained problem formulation. This approach can lead to unrealistic conclusions about OWN compared with traditional UWN designs.

The goal is to provide FAA stakeholders with evidence to gauge the intrinsic aero-propulsive (dis)advantages of OWN vs. UWN designs. It is impossible to pose a perfectly controlled experiment; however, we adopted a dual-parallel approach of optimizing OWN and UWN under the same MDAO formulation. This is an important decision in study methodology as it leads to a more controlled comparison and more credible conclusions.

Careful attention to valid OWN vs. UWN comparisons and numerical uncertainty thus informed much of the detailed work in our tasks, in hopes that such a research strategy would not lead to a simplistic performance comparison between the two configurations, but rather more credible and complex conclusions to inform FAA stakeholders about potential environmental impacts of each configuration.

Notation and Abbreviations
2-DoF: two-degree-of-freedom
α: angle of attack
ANN: artificial neural network
ANOPP: Aircraft Noise Prediction Program
C_D: drag coefficient

C_L: lift coefficient
CFD: computational fluid dynamics
CST: class function / shape function transformation
EDS: Environmental Design Space
FLOPS: Flight Optimization System
L/D: lift-to-drag ratio
MDAO: multidisciplinary design analysis and optimization
NPSS: Numerical Propulsion System Solver
O( ): order of magnitude
OEI: one engine inoperative
OWN: over-wing nacelle
pax: passenger [capacity]
UWN: under-wing nacelle

Task 1 - Creation of Single Aisle Aircraft Mission Model and a High Bypass Turbofan Propulsion Cycle Model

Objective(s)

The study focuses on the impact of an OWN installation on a 150 passenger ("pax") single-aisle aircraft. An aircraft mission model is needed to compute fuel burn and other responses for a typical mission. A cycle analysis is also required for this aircraft mission model to provide thrust, fuel burn, and other key quantities, as well as to solve a coupled problem with aerodynamics (CFD) through the exchange of boundary conditions. The aircraft mission model uses propulsion cycle analysis and some aerodynamic drag data from CFD to yield fuel burn.

Research Approach

This model is developed in the Environmental Design Space (EDS) framework (Kirby and Mavris 2008, Nunez, Tai and Mavris 2021) which integrates the engine cycle analysis code NPSS, an engine weight prediction tool WATE++, and the aircraft performance and mission analysis code FLOPS. The main ingredients for an aircraft model are as follows:

1. Development of an engine architecture model in NPSS
2. Selection of engine cycle design variables
3. Development of an airframe model in FLOPS
4. Specification of requirements such as a mission profile, desired range, cruise Mach number and altitude, etc.

The baseline engine selected for this vehicle is based off a notional Pratt and Whitney geared turbofan, specifically, the PW1100 series GTF. A general model of the mechanical design, geometry, and thermodynamics of the engine is created in NPSS using publicly available information. This model is then 'calibrated' to ICAO databank values of sea level static thrust and fuel flow, assuming that the calibration factors applied for that flight condition are valid throughout the operating envelope. The engine however is rubberized (Mattingly, Heiser and Pratt 2002), which means that the engine can be scaled up or down in thrust based on the results of the mission analysis, for a fixed thrust to weight ratio (T/W). The baseline T/W selected for this vehicle is 0.31, based on public information for the A320neo commercial transport airliner by AIRBUS Group, which is in the same passenger class considered for this study.

The preliminary mission analysis used FLOPS (Flight Optimization System), which is a NASA code. This model discretizes a mission into segments and enforces some conservation laws for a point-mass representation of the aircraft. Even though the conservation laws are applied on a point mass, the aircraft has attributes such as drag and engine performance data from internal models and external data tables that are based on physics/geometry inputs such as wing area, aspect ratio, etc. However, its formulation does not generalize well to more complex configurations with coupled lift and drag, as was found later.

The airframe model in FLOPS is built around the CFD geometry of the vehicle. The detailed geometry used for CFD is substantially based on the NASA Common Research Model (CRM). For example, the baseline airfoil stack is adopted from the CRM. However, conceptual-level sizing parameters were adopted from the A320neo because this aircraft model has been used previously in FAA-sponsored mission analyses.

Key variables like fuselage length, width, depth, wing planform area, aspect ratio, taper ratio, quarter chord sweep, and dihedral for example are matched between the CFD geometry and the FLOPS representation of this geometry. These variables impact the weight and aerodynamic performance predictions in FLOPS. The FLOPS aircraft model is sized for 150 passengers, at an assumed weight of 225 pounds per passenger (baggage + pax weight). The design range is specified to be 3415 nmi, with a cruise Mach number of 0.8 at 39,000 ft. A reserve mission for a 200 nmi trip to an alternate airport was also initially considered part of the requirements, though this reserve phase was excluded from the trajectory optimization results (presented in a later section) due to implementation challenges.

The mission analysis is initially conducted with FLOPS internal predictions for aerodynamics. The resulting engine dimensions and engine deck are then used to update the CFD model of the engine (both geometry and boundary conditions). RANS simulations of the airframe and engine (under-wing) are performed at cruise for an angle of attack sweep to generate a drag polar. A typical cruise part power condition is assumed to obtain the engine boundary conditions for this polar run. The resulting polar is then used to 'tune' the FLOPS internal aerodynamic predictions by adjusting FLOPS scaling factors on

parasitic drag and induced drag such that the cruise polar predicted by FLOPS matches the CFD generated polar. Following this tuning, EDS is re-run for the same inputs as before to determine a new engine size that meets the mission requirements. It is this new engine that is used for all subsequent CFD analyses on both OWN and UWN configurations.

It is important to emphasize that while EDS and CFD should theoretically be evaluated in a coupled manner till there is consistency between the engine used in the mission analysis and that used to generate the polars that feeds into the mission analysis, this iterative procedure is quite costly. As such, only a one pass update is used for establishing the vehicle model and the engine model in CFD. The main focus of this effort is to solve the aero-propulsive coupling problem within the CFD domain. *So, for a fixed engine size*, the goal is to match the engine operating conditions and inputs assumed by the NPSS model to those in the CFD domain through an iterative exchange of boundary conditions between the two disciplines. The engine size convergence between the NPSS model and that assumed in CFD is not closed. Table 1 and Figure 1 below summarize some key characteristics of the airframe and engine model.

Table 1. Summary of 150-pax aircraft model.

Name	Value
Fuselage Length (ft)	128.7
Fuselage Max Width (ft)	12.2
Fuselage Max Depth	12.2
Wing Planform Area (ft^2)	1642
Wing Aspect Ratio	8.4
Wing Quarter Chord Sweep (°)	33.76
Wing Taper Ratio	0.2
Wing Dihedral (°)	7.95
Design Payload (lb)	33,750
SLS Thrust/Engine (lb)	26,580
Thrust to Weight Ratio	0.31
Design Fan Pressure Ratio	1.525
Overall Pressure Ratio	47.91
Bypass Ratio	11.06
Design Range (nmi)	3451
Cruise Mach	0.8
Cruise Altitude (ft)	39,000

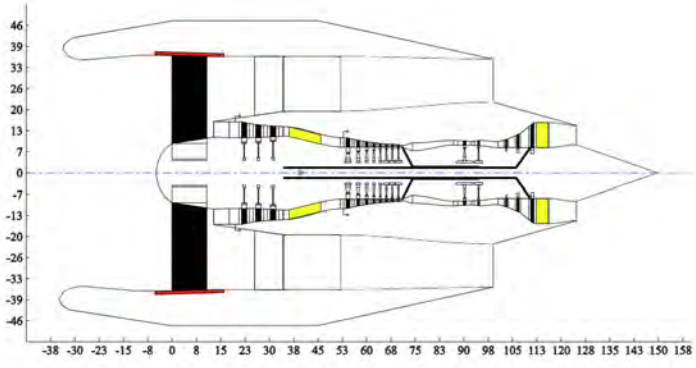

Weights		Dimensions	
Bare Engine Weight	4928.5	Engine Length	124.7
Accessories Weight	731.2	Engine Pod C.G.	39.5
Engine Weight	5659.7	Engine Max Diameter	72.6
Inlet/Nacelle Weight	89.4	Nacelle Max Diameter	0.0
Total Engine Pod Weight	5749.1	Total Engine Pod Length	124.7

Figure 1. WATE++ Outputs for the Final Engine Model Used in CFD (all dimensions are in inches and weights in pounds).

Milestone(s)

System level modeling to compute fuel burn and develop an engine model is complete.

Major Accomplishments
Baseline aircraft and engine models allow the propagation of aero-propulsion analysis to mission fuel burn and other system-level responses. An engine model was defined in terms of geometry and boundary conditions has been developed for use in CFD analysis of both the OWN and UWN configurations.

Publications
Ahuja, J., Lee, C, H., Perron, C., and Mavris, D. N., "Comparison of Overwing and Underwing Nacelle Aero-Propulsion Optimization for Subsonic Transport Aircraft," Journal of Aircraft, *Articles in Advance*, 2023, pp. 1-16 https://doi.org/10.2514/1.C037508

Outreach Efforts
None

Awards
None

Student Involvement
Jai Ahuja and Andrew Burrell contributed to the development of the baseline aircraft model.

Task 2 - Parametric Geometry Generation

Objective(s)
The solution to the MDAO problem involves the reduction of physics disciplines to functions such as f(**X**) where **X** is an array of design variables. An important and time-consuming preparatory step is to select candidate design parameters and create scripts through CAD or CAD-like software to generate water-tight geometry suitable for mesh generation. In the performance period, this parametric geometry effort focused on the outer mold line (OML) geometries of the fuselage, wing, and nacelles.

Research Approach
The selection of baseline aircraft mainly relied on two criteria: 1) applicability of the geometry to our current study of a single-aisle commercial airliner; 2) existing wind-tunnel/CFD data for such geometry in the public domain. By these two criteria, the NASA Common Research Model (CRM) (Vassberg, et al. 2008) was deemed as the most appropriate geometry available in the public domain. Since the CRM geometry was derived from a twin-aisle 300-passenger Boeing 777 design, it was determined that for the OWN problem, the baseline vehicle shall be a scaled-down version to match the overall dimensions of 150-passenger-class single-aisle Airbus A320neo aircraft.

To generate the fully parametric CAD model, the section data for the CRM fuselage, wing, horizontal tail, etc. were extracted from the original STEP file. Then the data was post-processed using Python-based scripts to make it import-ready for CAD model generation, which required the class function/shape function transformation (CST) parametrization (explained in later paragraphs) and data re-organization for generating closed profile sketches. Figure 2 shows the sections extracted from the STEP file.

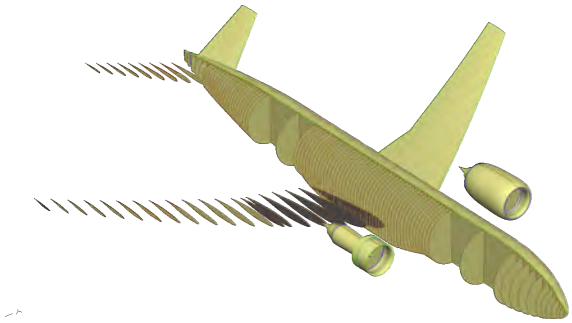

Figure 2. Cross-sections extracted from NASA CRM model for parametric model creation.

Implementation in Engineering Sketch Pad (ESP)

Two parametric geometry modeling tools were evaluated for this study: OpenVSP and Engineering Sketch Pad (ESP). Engineering Sketch Pad was chosen as the tool for this study mainly due to two advantages over OpenVSP: a) ESP's ability to design complex shapes and apply additional features to those shapes (e.g., blends and fillets) that are crucial in aerodynamic optimization studies based on CFD b) OpenVSP initially did not have interface to an adjoint feature in the inviscid CFD tool CART3D, which was the major drawback for its use in this study.

The ESP tool allows for a script-based bottom-up modeling approach to build complex CAD models using Constructive Solid Geometry concepts (Haimes and Dannenhoffer 2013). The tool generates complex geometries using feature trees and parameters commonly used in CAD software, allows for the creation of wire-bodies and sheet-bodies, is compatible with multiple operating systems, and uses a browser-based user interface. In the following subsections, we will discuss how various OWN baseline aircraft components were modeled in ESP.

Wing Design

The wing was modeled using airfoil sections extracted from the original CRM wing geometry and then lofting a surface through those sections, as shown in Figure 3. The airfoil geometry was specified using Engineering Sketch Pad's in-built Kulfan function which uses the class function / shape function transformation (CST) parametrization method (Kulfan 2008).

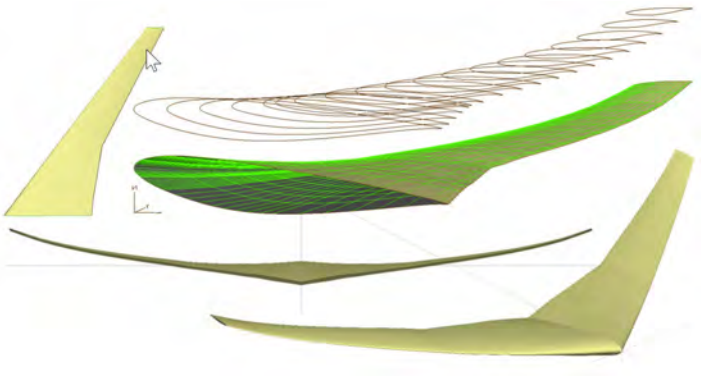

Figure 3. Example ESP output for wing.

The CST method allows for defining airfoil shapes using a simple analytic and well-behaved "shape function" that describes the geometry. The "shape function" provides the ability to directly control key geometry parameters that affect the airfoil drag, such as leading-edge radius, trailing edge boat-tail angle, and closure to a specified aft thickness. The shape function is mathematically represented by simple Bernstein polynomials, the coefficients of which become the parameters for controlling the airfoil shape (Tejero, et al. 2019). Therefore, the CST method requires relatively few variables to represent a large enough design space to contain optimum aerodynamic shapes for a variety of design conditions and constraints.

Initially, the wing was parameterized with one twist and eight CST coefficients (four each for the top and bottom of airfoils) at 21 spanwise stations. However, it was found that this parameterization allowed for physically unreasonable designs such as the exaggerated view in Figure 4.

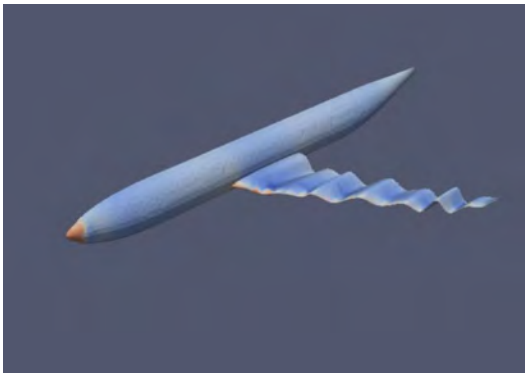

Figure 4. Example; parameterization method tries to limit such physically unreasonable cases in design domain.

In particular, this parameterization did not account for spatial correlation or dependence of design variables. For example, the twist in one spanwise station is highly correlated to its adjacent, neighboring stations. Therefore, the twist and airfoil CST coefficients were modified such that each parameter type across 21 stations is governed by a spline with control points. In later tasks, such as design variable screening and reduction, this spline parameterization was found to be much more efficient in terms of the fraction of feasible designs produced in sample domains.

Engine/Nacelle Design

The engine geometry was derived from approximating the overall dimensions of the Pratt and Whitney PW1000G engine family, which consists of high-bypass geared turbofan engines commonly seen on today's aircraft such as the Airbus A220, the Mitsubishi SpaceJet, the Embraer's second generation E-Jets, and as an option on the Irkut MC-21 and Airbus A320neo.

For CFD solver stability reasons, the engine bypass and core flows were modeled as annuli in CFD. The powered engine boundary conditions were implemented on surface patches in the end walls of the annuli and the flow was allowed to expand through channels. These channels are non-physical (i.e. not a realistic representation of actual engines) but are used to represent the exhaust flow. The main reason for this strategy is the numerical stability and robustness of the CFD solver setup across a wide range of nacelle designs and boundary conditions.

Particular geometry requirements arose because of this CFD strategy. The propulsion cycle analysis predicts properties, such as mass flows, which are linked to exit areas of the bypass and core streams using 1D governing physics equations. However, it is difficult to define a corresponding area in 3D or 2D axisymmetric CFD. The geometry was parameterized using Bézier curves such that there is a constriction near the exit from the bypass and core channels. This constriction was created such that the flow would choke (Mach = 1) close to the exit planes of the channels. This allows for the estimation of an exit area that corresponds to the nozzle exit area in propulsion cycle analysis.

These geometry modeling decisions are not without drawbacks. In particular, there are difficulties in defining design domains *a priori* that would produce physically reasonable geometries. For example, if the tail cone angle is steeper (narrowing to a point sooner), then the outer wall of the bypass annulus (underside of the outer nacelle "airfoil") must be correspondingly deflected inward to avoid large regions of separated flow. Yet, this requires accompanying changes near the trailing edge of the outer "airfoil" for geometric compatibility. This can cause failed geometries or at least highly unfavorable aerodynamic designs. The nacelle parameterization was thus a compromise between the robustness of the CFD, ease of propulsion-aerodynamics integration, and the desire to yield feasible/reasonable geometries for much of the design space. Figure 5 shows the finished engine geometry ready for CFD simulation.

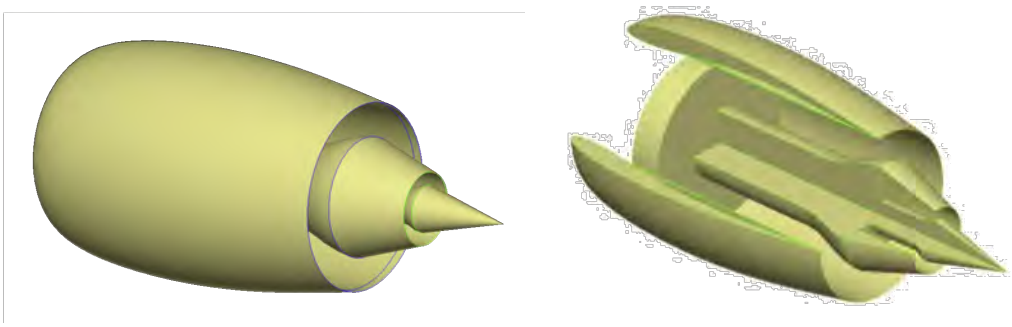

Figure 5. Fully Parametric OWN Engine Geometry generated in ESP.

Fuselage/Horizontal Tail Design

A process similar to the wing design process was used to model the horizontal tail and the fuselage of the aircraft, i.e., by generating sketches from extracted section data and then lofting a surface through those sketches to generate the final geometry. As described earlier, the OWN aircraft geometry is a scaled-down version of the original CRM geometry. Figure 6 depicts the complete CRM aircraft before and after the scale-down process. The horizontal tail was eventually not used in the CFD models and instead an extra drag term was added to the CFD predicted drag to account for the empennage.

Figure 6. Side-by-side comparison of the Original NASA CRM aircraft and scaled-down version of the OWN baseline aircraft (modeled in ESP). Top view (Left) and front view (Right). The scale factor is 60.2% for the fuselage, 60.9% for the wing, and 62.25% for the horizontal tail (scaled with respect to longest dimension).

High Lift Surfaces Design

High lift geometry variant of the parametric wing geometry was produced by first extracting the data from the NASA CRM High Lift Prediction Workshop 5 (HLPW5) clean geometry. This geometry, pictured in Figure 7, has slightly different airfoil sections at the leading edge as compared to the original NASA CRM geometry, as well as a lack of wing bending effects to allow for ease in manufacturing wind tunnel models for high lift surfaces (Lacy and Sclafani 2016). Once the clean geometry was generated, the high lift surfaces were extracted based on the geometric variables as outlined in the reference paper (Lacy and Clark 2020). In particular, slat and flap kinematics were modeled by running a MATLAB-based optimizer script that satisfies the constraints for the input variables gap, height and deflection for slat and gap, overlap and deflection for inboard and outboard flaps. In particular, linkages and fairings were not modeled to avoid incurring additional computational costs during mesh generation and CFD execution. The final geometry matches the complexity of High Lift Prediction Workshop 3 (HLPW3) geometry, with four main elements: main wing, one slat, and two flaps, as seen in Figure 7.

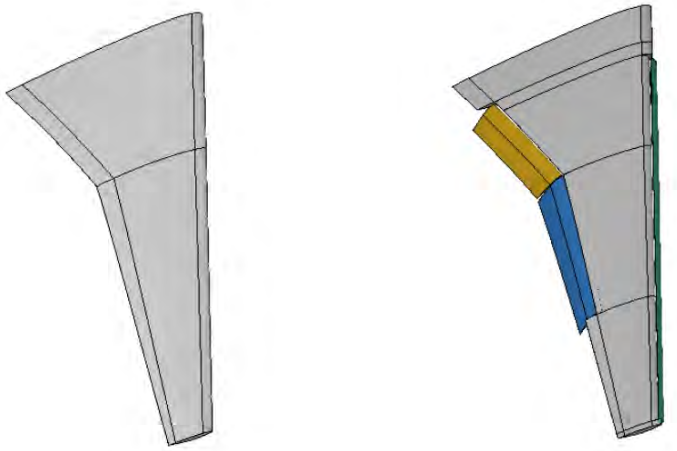

Figure 7. Fully Parametric High Lift Wing Geometry generated in ESP. The clean geometry (left) was first generated by replicating NASA HLPW5 model. Using this model as the baseline, high lift surfaces are extracted (right) based on the high lift design parameters.

Milestone(s)
The reference airframe and the engine geometry were parametrically modeled and are ready for CFD simulations.

Major Accomplishments
A baseline aircraft design was successfully created based on reduction of the NASA Common Research Model. Aircraft wing and nacelle design variables were parameterized and implemented in Engineering Sketch Pad scripts.

Publications
None

Outreach Efforts
None

Awards
None

Student Involvement
Salah Tarazi (PhD student at the time) played a major role in adapting the NASA CRM and implementing the baseline vehicle geometry in Engineering Sketch Pad. Stephanie Zhu (PhD student at the time) was involved in wing parameterization in Engineering Sketch Pad and its linkage to CFD software.

Task 3 - Formulate MDAO problem

Objective(s)

The overall goal was to state a multidisciplinary analysis and optimization (MDAO) (Martins and Lambe 2013) problem to assess a single aisle OWN transport aircraft. The MDAO process was originally intended to use CFD, noise analysis codes such as ANOPP, as well as weights, engine cycle, and mission analysis. The formulation evolved during the project in light of the results. The original statement of the problem:

- **Minimize**: fuel burn
- **Subject to**: design requirements including aircraft range, and detailed side constraints such as wing/tail ground strike and tip-over requirements
- **With respect to**: design variables including engine nacelle position (focusing on forward placement), nacelle and wing geometry, engine cycle and operating condition
- **Given**: baseline single-aisle aircraft model and mission profile

In discussions with FAA technical advisors, more emphasis was placed on optimizing aerodynamic performance rather than noise, which is necessarily of lower fidelity. The single objective function of steady-state fuel burn in cruise was to be minimized with respect to geometry and propulsion variables, with total mission fuel burn computed as a secondary response using a newly developed mission analysis capability, though noise was evaluated as a response at certain design points.

Given this general MDAO problem, a large portion of the task focused on providing more detailed definition to the aero-propulsion aspect of the MDAO formulation.

Research Approach

One of the most computationally intensive aspects of the MDAO is the aero-propulsion coupling problem. The aerodynamics discipline uses results from the propulsion cycle analysis (the NPSS code) as boundary conditions, and vice versa. A valid MDA solution is found only when these coupling variables, which are shared between disciplines, converge to a consistent value. There are different MDA methods to achieve such interdisciplinary closure, and they have different costs in the number of function calls. Therefore, this effort focused on the most important aero-propulsion aspects of MDAO, which drive the overall architecture of the problem. Noise and detailed side constraints mentioned above are important, as they allow solutions to capture realistically important physics trade-offs such as the noise reduction due to shorter landing gears enabled by over-wing engines. However, those constraints were never incorporated into the final MDAO formulation.

In research such as this, each CFD simulation could cost at least O(1000) core-hours, so it was important to minimize the number of iterative function calls to converge a single MDA. The overall MDAO design problem had constraints related to physical equilibrium. These were restated as equality constraints for interdisciplinary consistency:

- Core flow consistency: $h_1 = \left|W_7^{NPSS} - W_7^{CFD}\right| \leq \epsilon_1$
- Bypass flow consistency: $h_2 = \left|W_{17}^{NPSS} - W_{17}^{CFD}\right| \leq \epsilon_2$
- Inlet pressure recovery consistency: $h_3 = \left|\eta_{PR}^{NPSS} - \eta_{PR}^{CFD}\right| \leq \epsilon_3$
- Streamwise force balance: $h_4 = \left|\sum F_x^{CFD} + F_x^{FLOPS}\right| \leq \epsilon_4$
- Stream-normal or lift force balance: $h_5 = \left|C_L^{CFD} - C_L^{Target}\right| \leq \epsilon_5$

Here, W is the weight (or mass) flow, with subscripts 7 and 17 indicating engine stations equivalent to the CFD boundary condition for exhaust flow. F_x^{FLOPS} is the streamwise force contribution from empirical drag models for components other than the wing-body-nacelle modeled in CFD. All of these constraints h_i were set to small tolerances ϵ_i.

Several MDA methods were tested with different levels of geometric complexity before selecting a final MDA method. Initial research focused on a relatively simple, 2-D axisymmetric, isolated nacelle to test MDA strategies using a subset of the above constraints h_i. For example, a simple, looping method (Gauss-Seidel) was used in Figure 8.

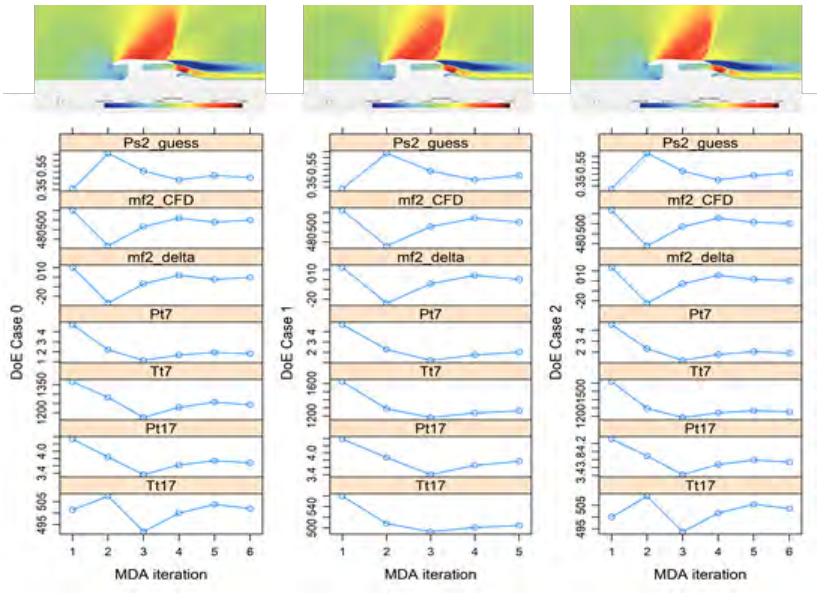

Figure 8. Example convergence history of aero-propulsion coupling variables for three design cases of a 2-D/axisymmetric nacelle.

During the course of this research, we realized an important potential discrepancy between NPSS propulsion cycle assumptions and CFD boundary conditions. The "0-D" NPSS code does not spatially discretize flow equations but rather connects analytic/empirically tuned flow equations for different turbomachinery elements at different stations in the engine. For example, at a nozzle station, 1D isentropic nozzle flow equations (with any tuning factors) can be used along with entry/exit areas to yield a solution coupled with all other cycle elements.

This nozzle element is of interest. In typical propulsion cycle analysis, it is assumed that the nozzle exhausts a flow to external flow conditions, typically free-stream conditions. However, the nozzle exit flow may not actually reach free-stream conditions at the nominal outlet location and area. In Figure 9, it can be seen in an example CFD case that the bypass and core exhaust streams may not reach free-stream pressure at their respective, nominal "A_8" and "A_{18}" exit areas.

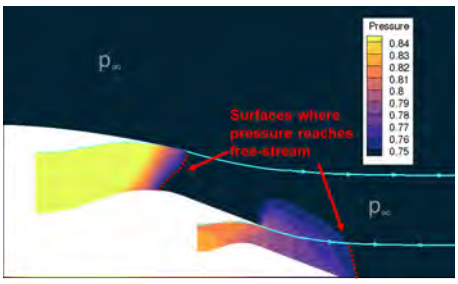

Figure 9. Areas at which exhaust streams reach free stream pressure can be significantly different from nominal bypass and core exit areas.

This led to a physics inconsistency between cycle analysis and CFD which was considered as essentially internal and external aero-thermal analyses which must pass consistent information over boundary conditions. The situation was furthered complicated in forward-mounted OWN applications because the presence of a wing aft of the engine strongly affects the exhaust flow compared to the isolated engine assumed in NPSS.

Figure 10. Mach contour plot shows influence of wing on exhaust streams of engine.

A major development was to adjust the aero-propulsion MDA problem to enforce the consistency constraints shown earlier by manipulating fictitious "exit areas" A_8 and A_{18} in the propulsion cycle. This is tantamount to an iterative CFD-based calibration of NPSS model to account for complex OWN aero-propulsive interactions.

We tested several different MDA and MDAO architectures to find a method that efficiently enforces the above MDA equality constraints, h_1, h_2, …, h_5. For example, Figure 11 shows a snapshot of a Bayesian adaptive sampling approach based on (Lee and Mavris 2012) that progressively learns the settings for coupling variables that most likely satisfy the constraints.

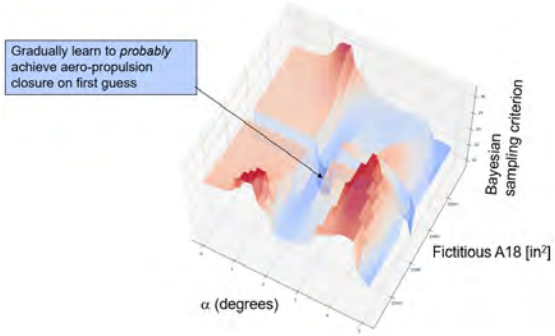

Figure 11. Bayesian method showing coupling variable domain regions with high probability of MDA closure.

We finally selected a simple method based on the commercial STAR-CCM+ CFD code's macro scripts. This was an intrusive alteration of the CFD solution process to enforce the MDA constraints. Surrogate models of NPSS were created and included inside the CFD solver script. While the CFD code iteratively solves its governing equations with respect to the flowfield state variables, it also manipulates coupling variables by querying the NPSS surrogates until MDA closure is achieved.

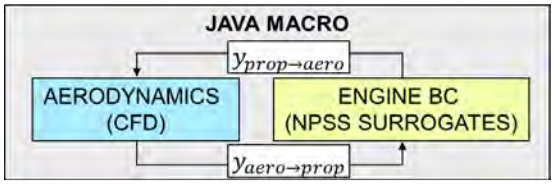

Figure 12. Final aero-propulsion coupling method: solver macros intrusively enforce MDA consistency within the CFD code.

Reducing Dimensionality of the Problem

The external shape of aerodynamic bodies, such as wings and nacelles, is characterized by complex and detailed surfaces. In turn, the definition of these surfaces necessitates many design parameters. This design problem contained a total of 44 variables which are listed in Table 1. This large number of design variables hinders the design exploration of the aircraft design due to a phenomenon referred to as the *curse of dimensionality* in machine learning literature. Therefore, to effectively tailor the airframe for a given engine location, some steps must be taken to bring down the dimension of the design space to a more reasonable value.

Table 2. List of original design variables before reduction.

Group	Variable Name	Dimension
Nacelle	Highlight lip radius	1
	Cowl maximum radius	1
	Cowl maximum radius location	1
	Cowl trailing edge angle	1
	Cowl trailing edge curvature	1
	Inlet throat location	1
	Nacelle X location	1
	Nacelle Z location	1
Wing	Wing CST coefficients (upper surface)	16
	Wing CST coefficients (lower surface)	16
	Wing twist distribution	4
	Total	**44**

For the current problem, the dimension of the design space is reduced using the active subspace method as described in (Constantine 2015), which is a type of supervised dimensionality reduction technique. Assuming a generic function that depends on many inputs, this method identifies a linear subspace of the input spaces which is responsible for most of the variability of the function. The active subspace is defined using an orthogonal basis whose vectors represent a linear combination of the original design variables. Designs in the original space can then be projected into the active subspace, and the resulting coordinates are called active variables. Note that the transformation from the active variable to the original design variables is also straightforward as it only requires the transpose of the computed orthogonal basis. Conceptually, one can also consider the active subspace as a rotated set of axes in the design space for which the function variation is best captured as shown in Figure 13.

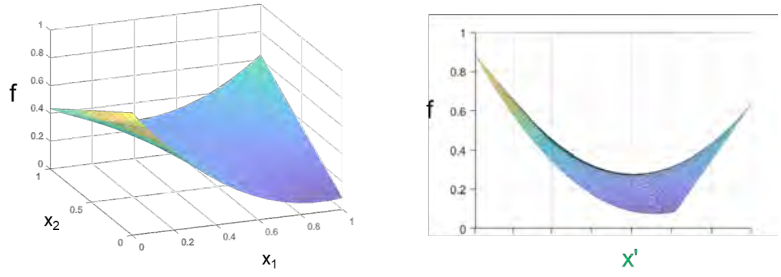

Figure 13. Notional view of active subspace for two original design variables (left).
The rotated view (right) shows that a single new variable x' captures important features of function f.

The classical active subspace method requires the computation of the gradient of the function of interest. However, in the last few years, some authors have proposed alternative methods that can extract the subspace in a gradient-free manner. One of these methods is the manifold optimized active subspace (MOAS) which was initially proposed by (Tripathy, Bilionis and Gonzalez 2016) and improved by (Rajaram, et al. 2020). Specifically, the MOAS method uses a Gaussian process (GP) to link the function inputs and outputs, and the active subspace is obtained by maximizing the likelihood of the GP via a manifold optimization algorithm. While the analysis tools used in this work can provide gradient information, the airframe uses the gradient-free MOAS approach. This decision was motivated by the additional computation cost of computing the gradient and initial testing that showed noise in the gradient results which negatively impacted the accuracy of the active subspace. Note that the MOAS results are computed using the framework developed by (Gautier, et al. 2022), which is openly available[1].

[1] Source code available at https://gitlab.com/raphaelgautier/bayesian-supervised-dimension-reduction

Additionally, while the active subspace method can facilitate the exploration of a high-dimensional design space, a substantial amount of training data must still be generated initially. This can be quite costly when used in combination with high-fidelity RANS simulations. As such, to further reduce the computational cost of the design exploration, the active subspace in this work is computed using inviscid results obtained with Cart3D CFD software. The computed subspace is then used directly for the generation of RANS results. While the inviscid active subspace is likely different than the RANS one, the difference between the two is assumed to be relatively small since the aerodynamic performance of the aircraft is expected to depend strongly on inviscid effects such as shock waves and induced drag. The potentially lower accuracy is also compensated for by the inexpensive generation of inviscid data.

Scope of Design Variables

The parameterization of geometric design variables is covered separately, but the MDAO formulation effort provided bounds for the scope of optimization. In consultation with FAA technical advisors, the NASA Common Research Model (CRM) was chosen as a baseline geometry (Vassberg, et al. 2008). Many parts of the aircraft geometry were deemed to be out of scope for the present research. Other than scaling from 300 to 150-passenger size, the fuselage is fixed. The justification for these decisions is an emphasis on credibility and reproducibility in the main research goal: a comparison between under-wing and over-wing nacelle configurations. In actual practice, an aircraft outer mold line (OML) geometry may involve thousands of detailed design variables, many more physics disciplines, flight scenarios, and constraints. For example, one consequence of simply scaling the fuselage shape is that the cockpit windows are much smaller. It is unlikely that pilot visibility requirements simply scale linearly with a fuselage length scale. Yet, this simple scaling of the CRM geometry is easily understood and replicable by the wider aeronautics research and industry communities. It avoids arbitrary detailed design decisions by the researchers.

Because of this concern with credible and replicable comparison, several other parts of the aircraft geometry are not included in the MDAO study. The empennage requires flight mechanics and detailed mass estimation (ex: trimming the horizontal tail plane requires knowledge of the center of gravity). Therefore, it is not included in high-fidelity simulation, although mission analysis included friction drag of the empennage via the detailed aero-propulsion surrogates. The landing gear pod region is not modified. The wing airfoils design space is constrained to a relatively small domain such that the structural thickness is not radically altered. The wing planform is also fixed.

The current approach is to not design a pylon joining the wing and nacelle, even though it undoubtedly plays an important role in interference drag for an over-wing nacelle. Because the present effort includes no structural or thermal analysis, the pylon geometry would involve many potentially unrealistic guesses. To give decision-makers a fair assessment of the potential benefits of OWN installation, we argue that a comparison of OWN and UWN should be made with no pylons or with thin placeholder/default pylons based on similar geometry rules for the two cases.

Finally, one of the most important variable scoping decisions is to limit the study to the forward placement of nacelles. This decision was made in discussions with the FAA and was driven by interest in the noise shielding effect from the wing. A nacelle aero-propulsive optimization was initiated for rearward placement after the main period of performance ended, but not incorporated into the mission analysis.

Adaptive Sampling Optimization

The main optimization was performed with a Bayesian adaptive sampling technique. It sequentially fit a Gaussian Process or Kriging model and added new sample points according to an acquisition function or infill criterion. In our case, we used the expected improvement (EI) infill criterion. EI has been described in literature such as (Jones, Schonlau and Welch 1998) and is shown notionally in Figure 14 below. This procedure was carried out until the EI was of a similar order of magnitude as the numerical uncertainty due to the CFD grid (described in a later section).

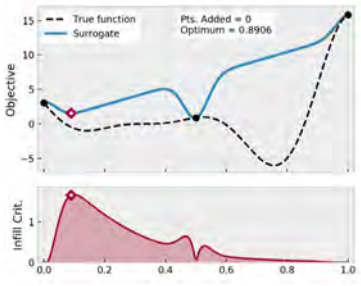

Figure 14. Snapshot of an adaptive sampling process. The infill criterion is maximized to identify the most favorable location for evaluating a sample point.

Milestones

- Various methods tested for aero-propulsion coupling:
- Direct multi-disciplinary feasible (MDF) method tested on 2D axisymmetric, isolated nacelles
- Direct multi-disciplinary feasible (MDF) method tested on full aircraft
- Rejection sampling method tested using 3D nacelle and wing (no fuselage)
- Bayesian adaptive sampling method tested for 3D nacelle and wing
- Fully coupled, intrusive method tested with full aircraft wing-body-nacelle.
- Active subspace methods compared and selected

Major Accomplishments

- Draft of a Design Structure Matrix (Lambe and Martins 2012) and variable breakdown for geometry-integrated MDAO.
- Formulation of MDAO problem in terms of disciplinary analyses available and under development, scoped down according to sponsor interest and feasibility of implementation.
- Aero-propulsion MDAO method selected and implemented: fully coupled method implemented to incorporate propulsion cycle surrogate models within CFD macro solver scripts
- Active subspace variables used successfully in design study

Outreach Efforts

None

Awards

None

Student Involvement

Kenneth Decker and Bilal Mufti were PhD students at the time who contributed by testing different MDAO formulations on reduced order or inviscid test cases. Bilal Mufti and Mengzhen Chen tested different MDA architectures using CFD and NPSS propulsion cycle analysis.

Publications

Ahuja, J., Lee, C, H., Perron, C., and Mavris, D. N., "Comparison of Overwing and Underwing Nacelle Aero-Propulsion Optimization for Subsonic Transport Aircraft," Journal of Aircraft, *Article in Advance*, 2023, pp. 1-16 https://doi.org/10.2514/1.C037508

Outreach Efforts

None

Awards

None

Task 4 - Generation of CFD Templates and Automation Scripts

Objective(s)

In order to solve an MDAO problem, the workflow between the geometry generation to the CFD solution and post-processing must be reduced to a robust function call. CFD meshing in particular is difficult to automate as a "fire-and-forget" process without human inspection or intervention. Yet, a high degree of automation is needed to allow modern design techniques such as active subspace, adaptive sampling, and multi-fidelity methods. This detailed development work may be of less interest to the stakeholder or decision-maker, but it is identified as a separate task because it accounts for a large share of actual effort and calendar time. The goal of this task is also to generate CFD grids of different resolutions and compare the solution for accuracy. Also, the impact of the accuracy on the fuel burn calculations was quantified. The results were used to guide MDAO convergence criteria such that the optimization is not continued beyond the uncertainty "floor" of the physics analysis.

Research Approach

In the example below in Figure 15, an off-line design of experiments (DoE), or sample specification, is used as a placeholder for an MDAO driver or optimizer.

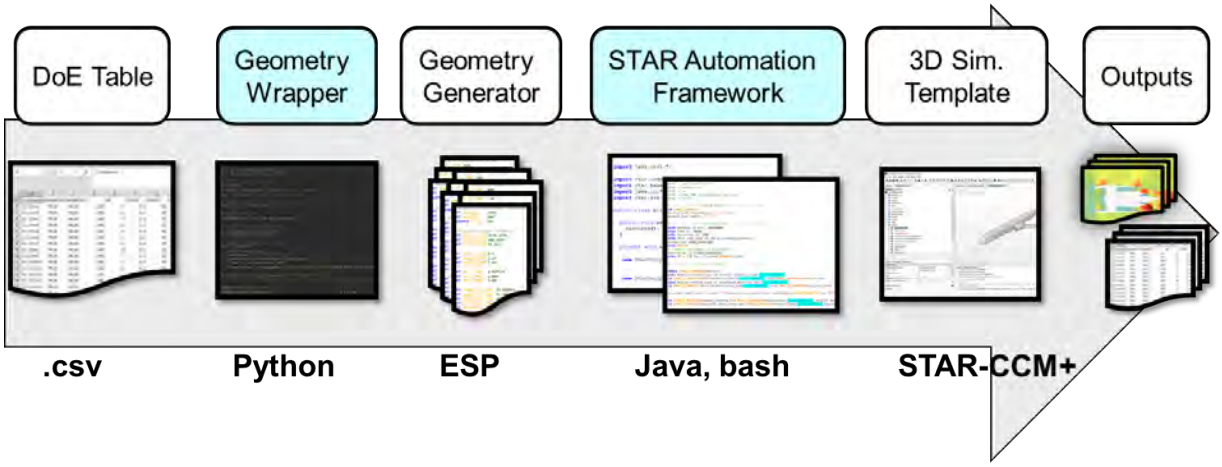

Figure 15. Automated workflow for example design activity (design of experiments, or DoE).

STARCCM+ Reynolds Averaged Navier Stokes CFD solver was used for this optimization study. STARCCM+ in-built unstructured grid generator was used to generate hybrid volume mesh containing orthogonal prismatic cells, also known as prism cells, near the surface to resolve the boundary layer and polyhedral cells for the remaining volume mesh. Through the literature survey, it was found that previous OWN configuration optimization studies have meshes ranging from 0.8M to 30M cells (Fujino and Kawamura 2003, Hill, Kandil and Hahn 2009, Renganathan, et al. 2018). Therefore, for the current study, a detailed grid sensitivity analysis was performed before finalizing the grid to establish a reference uncertainty floor. The six grids (see Table 3) that were used ranged from the coarsest size of 19.5M cells to the finest size of 475M cells, with the latter being used as the reference case to compare the accuracy. The net *L/D* calculation error for all cases compared to the reference case was within 2% for the coarsest grid. Based on the findings, the 76M grid was chosen for the optimization study.

Table 3. Grid Convergence Study Results.

	CFD Mesh Cell Count					
	19.5M	33M	76M	161M	303M	475M (Reference)
% *L/D* Error	1.955	1.495	0.476	-0.329	0.179	0

The CFD error in drag computations associated with different grid sizes was propagated to mission fuel burn change (Figure 16) in a rapid estimate. The study was carried out using a modified version of FLOPS which allows user-specified data tables for the aerodynamic model of the aircraft. Results are in Table 4. As before, the change in drag coefficient (ΔC_D) for only the cruise condition was obtained for all cases by keeping the drag value obtained for the 475 million cells grid as the baseline. For a rough estimate of the uncertainty impact of CFD mesh-related error, the ΔC_D was applied to the empirically-based aerodynamics models of FLOPS. The drag polar for the complete aircraft at different flight conditions was computed using empirical drag estimation techniques (EDET). This baseline drag polar was perturbed by adding ΔC_D using a blending function such that the change in drag is maximum at flight conditions at which ΔC_D was computed and decreases linearly as the Mach number is changed.

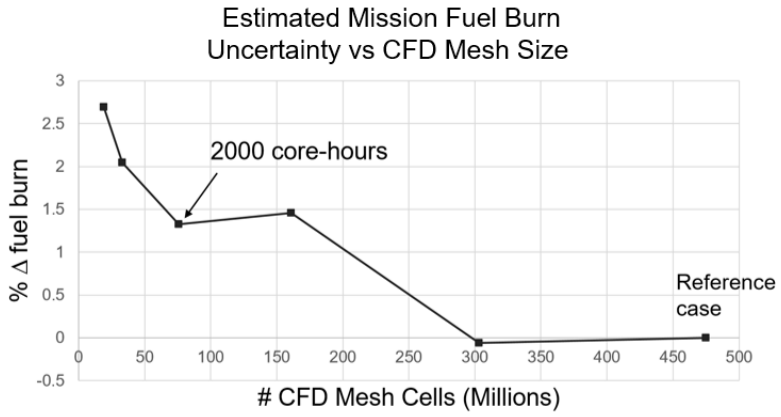

Figure 16. Mission fuel burn change associated with CFD data generated on meshes of various sizes.

Table 4. CFD error propagation to Mission Fuel Burn Calculations.

Grid Size (Millions)	ΔC_D	Estimated % Discrepancy in Mission Fuel Burn
19.5	6.78E-4	2.69
33	5.19E-4	2.05
76	3.37E-4	1.32
161	3.72E-4	1.46
303	-0.154E-4	-0.06
475 (Reference)	**0**	**0**

When examining the CFD solutions, there are often only subtle physical differences in flowfields. For example, there is over a 2% discrepancy in estimated mission fuel burn for the two mesh settings below in Figure 17. However, note that much of the recently published OWN literature may be qualitatively similar to the coarser of these two extremes.

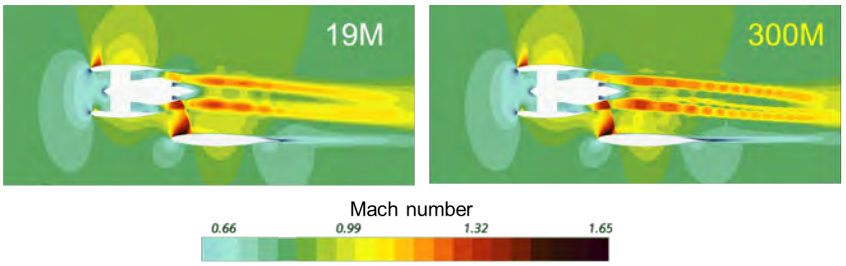

Figure 17. Subtle differences in flowfields of different mesh cell counts associated with mission fuel burn discrepancies.

Milestone(s)
A mesh sensitivity study was completed.

Major Accomplishments
Initial automation of 2D axisymmetric CFD nacelles contributes to development of screening/variable reduction methods and MDAO techniques in later tasks. Uncertainty impact of CFD mesh propagated to uncertainty in system-level metric — fuel burn.

Publications
Ahuja, J., Lee, C, H., Perron, C., and Mavris, D. N., "Comparison of Overwing and Underwing Nacelle Aero-Propulsion Optimization for Subsonic Transport Aircraft," Journal of Aircraft, *Article in Advance*, 2023, pp. 1-16 https://doi.org/10.2514/1.C037508

Outreach Efforts
None

Awards
None

Student Involvement
Salah Tarazi played a major role in adapting the NASA CRM and implementing the baseline vehicle geometry in Engineering Sketch Pad. Stephanie Zhu was involved in wing parameterization in Engineering Sketch Pad and its linkage to CFD software. PhD student Bilal Mufti propagated the CFD numerical uncertainty through the mission analysis to estimate fuel burn impact.

Task 5 - Stage 1 Design: Nacelle and Wing Optimization (Forward Mounted OWN)

Objective(s)

As discussed previously, the overall goal was multidisciplinary analysis and optimization (MDAO) of an OWN aircraft. This was scoped down over the course of the project to exclude noise from the MDAO problem, and the focus narrowed to coupled aero-propulsion CFD and cycle analysis to inform a mission analysis (further described in a later section). The working MDAO problem statement may be expressed as:

- **Minimize**: fuel burn for a baseline mission
- **Subject to**: range and detailed side constraints
- **With respect to**: design variables including engine nacelle position (focusing on forward placement), nacelle and wing geometry, engine operating condition
- **Given**: baseline single-aisle aircraft model and mission profile
- **Returning**: fuel burn

In discussion with FAA technical advisors, more emphasis is placed on aerodynamic performance optimization rather than noise, which is necessarily of lower fidelity. So, the single objective function of fuel burn is minimized, though noise was evaluated for specific settings of design variables (see section on noise studies). To control the "curse of dimensionality," the stage 1 optimization process was broken into two steps. The first step focused on the commitment of nacelle location before more detailed shape optimization in step 2.

Research Approach

We focused first on the nacelle location relative to the wing-body in the *X-Z* plane, at a fixed span-wise *Y* location. Figure 18 below shows examples of how the nacelle location was varied. The black dots show positions of a reference a point on the nacelle. The 3x5 grid of black dots were sampled with the results shown in Figure 19. The blue nacelles are closest to the wing, and the grey nacelles are farthest. We selected the orange cases as final locations for second-stage, detailed optimization.

We note that the selection of these orange cases was highly subjective, especially for the OWN case, but were made in consultation with FAA advisors. We emphasize that this was an arbitrary, human decision. But this is not a result of ignorance of rigorous optimization methods; rather, it is an unavoidable consequence to focusing on an aero-propulsion physics scope. The results showed that fuel efficiency at cruise improves as the nacelle moves farther away from the wing. This is a consequence of the reduced MDAO problem statement that does not include a structures/weights discipline. In a larger scale, more realistic problem, the structural weight and drag of pylon as well as wing structure would penalize nacelle placements far from the wing.

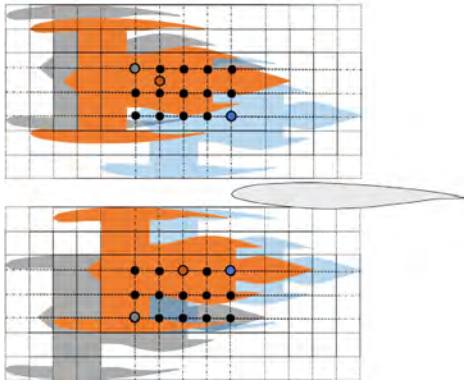

Figure 18. Orange locations are final selections for OWN and UWN.

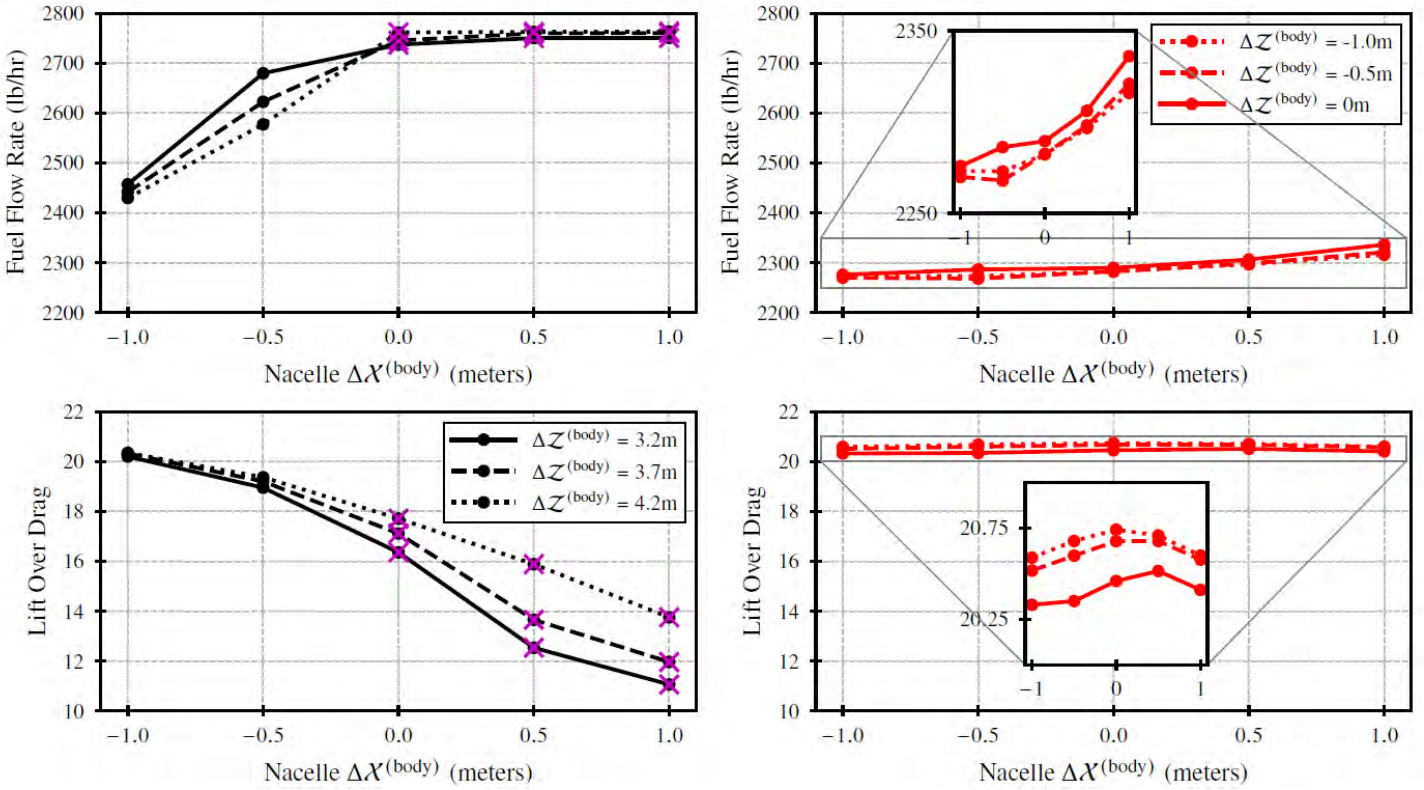

Figure 19. Results of the Nacelle Perturbation Study.

There are few publicly available empirical pylon weight values, so we referred to physics models used in MDAO studies for order-of-magnitude estimates. For example, Gazaix and colleagues report an optimized pylon mass of roughly 700 kg for a similar class of aircraft (Gazaix, et al. 2019). Perturbing weight values in our baseline FLOPS mission analysis (not the mission analysis used for final optimized trajectories as discussed later) showed order-of-magnitude sensitivities of O(1%) change in mission fuel burn due to O(1000 lbf) aircraft weight perturbation. It is difficult to guess precisely how the pylon mass increases with nacelle distance from the wing attachment points, but it is reasonable to assume the weight increases at least proportionally (Or even higher) with increases in this distance. Therefore, we roughly estimated that doubling the pylon length has O(1%) mission fuel burn impact. With this in mind, we selected arbitrary intermediate nacelle locations for further refinement.

After down-selecting a nacelle location, we then focused on more detailed shape optimization of the nacelle and wing. We used a gradient-free active subspace technique to reduce 44 wing and nacelle shape variables to 7 active modes or hybrid design variables that captured the major features of the original variables, as discussed in a previous section. We show theoretical details of this technique for aerodynamic examples in a conference paper (Mufti, et al. 2022). For optimization of the active variables, we used a kriging or Gaussian process-based adaptive sampling method to minimize fuel flow rate at cruise (Mach 0.8, 39,000 ft). The procedure is a variant of a common expect improvement or "efficient global optimization" (EGO) method described by (Jones, Schonlau and Welch 1998).

Note that this is a reduced/approximate version of the overall problem statement of minimizing fuel burn over an entire mission. The adaptive sampling continued until the expected improvement in fuel flow fell within the uncertainty in the coupled aero-propulsion analysis.

Results of analyses of the propulsion and aerodynamics optimized designs are shown below in Table 5.

Table 5. Stage 2 optimization results.

Parameter	Baseline OWN	Optimized OWN	Baseline UWN	Optimized UWN
Fuel flow rate (lb/h) at cruise	2600	2330	2290	2240
L/D	19.3	21.5	20.5	21.3
Power code (throttle)	48.3	45.4	44.9	44.4
Pressure recovery	0.9965	0.9975	0.9975	0.9976

Surface pressure contours for baselines and optima for the two cases are shown below in Figure 20. In both cases, there are significant shocks between the nacelle and fuselage. The shocks are slightly weakened but the differences are visually difficult to discern in the color maps. For OWN, the shock over the nacelle weakens substantially and moves aft. This is related to an increased maximum radius near the highlight for the optimized OWN.

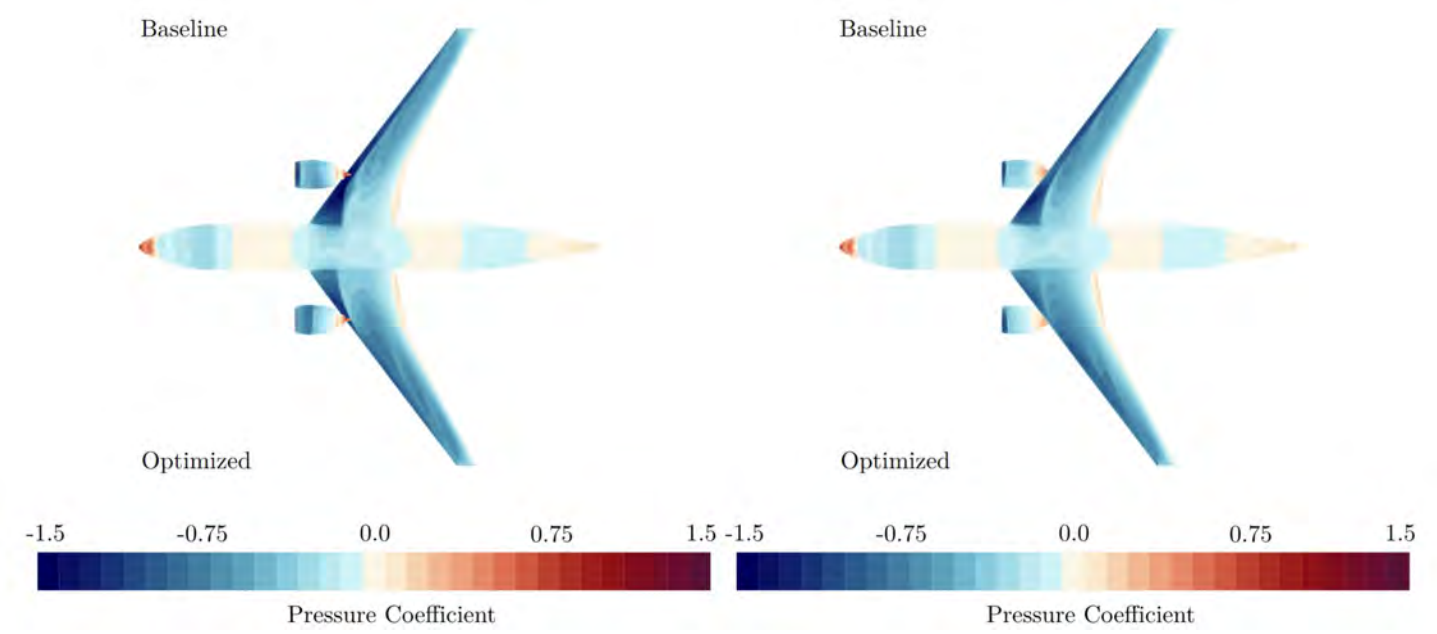

Figure 20. Pressure contours shown for OWN baseline and optimum (left) and UWN (right).

The analysis shown here corresponds to an OWN design with a 4% higher fuel flow rate than UWN, but we avoid broad conclusions or generalizations from this result. This study deliberately aimed to control many factors to first compare the effect of moving an engine of fixed size between the two configurations.

Major Accomplishments

Estimates were provided of realizable performance for a grid of nacelle positions. Baseline nacelle locations for OWN and UWN were selected in discussion with FAA technical advisors. Optimization and comparison of OWN and UWN at cruise conditions was completed for a fixed engine cycle and size. Final configurations were used to produce aero-propulsion data for training surrogate models used later in mission analysis.

Publications

- Bilal Mufti, Mengzhen Chen, Christian Perron and Dimitri N. Mavris. "A Multi-Fidelity Approximation of the Active Subspace Method for Surrogate Models with High-Dimensional Inputs," AIAA 2022-3488. AIAA AVIATION 2022 Forum. June 2022.

- Ahuja, J., Lee, C, H., Perron, C., and Mavris, D. N., "Comparison of Overwing and Underwing Nacelle Aero-Propulsion Optimization for Subsonic Transport Aircraft," Journal of Aircraft, *Article in Advance*, 2023, pp. 1-16 https://doi.org/10.2514/1.C037508

Outreach Efforts
Researchers collaborated with NASA over-wing nacelle expert during regular telecons.

Awards
None

Student Involvement
Mengzhen and Bilal Mufti were PhD students at the time who contributed by testing different MDAO formulations using coupled propulsion cycle and CFD analyses.

Task 6 - Create ANOPP Noise Models

Objective(s)
One of the main anticipated benefits of the OWN configuration is noise shielding from the wing. Despite the importance of modeling noise, high fidelity physics modeling is out of scope for this present project due to the complexity and computational cost of analysis. Rather than a direct objective function in optimization, a lower order analysis is used to model noise (originally considered as a constraint but later simply evaluated as a response) while optimization focuses on aero-propulsion responses. The goal of this task was to use a noise analysis code, such as the Aircraft Noise Prediction Program (ANOPP), to generate approach, cutback, sideline, and cumulative noise data via a design of experiments, thereby allowing surrogate models to be fit to the data set to predict changes in aircraft noise due to nacelle location.

Research Approach
Acoustics are modeled using a lower fidelity mode of ANOPP software. The NASA Aircraft Noise Prediction Program (ANOPP) code (Zorumski, ANOPP Theoretical Manual, Pt. 1 1982, Zorumski, ANOPP Theoretical Manual, Pt. 2 1982) is used to model engine noise as a single source. Because of the relatively coarse spatial representation of noise, it is assumed that the dependence of noise responses with respect to nacelle geometry placement are crude at best. ANOPP is selected as a suitable noise analysis code based on the required level of detail and tools available to the researchers.

Nonetheless, keeping the above caveats in mind, initial configuration studies addressed the following questions:
- Does the aft engine noise dominate the conversation moving forward?
- How much benefit does shielding provide for the forward mounted configuration?

A preliminary study was conducted by decomposing forward-radiated vs. aft-radiated engine noise. The engine was simply moved above and below the wing by up to +/- 1.38 nacelle diameters for a baseline engine geometry. Comparisons were made for different technology assumptions (corresponding to years 2017, 2027, 2037) for sideline and cutback noise. An example result is shown in Figure 21.

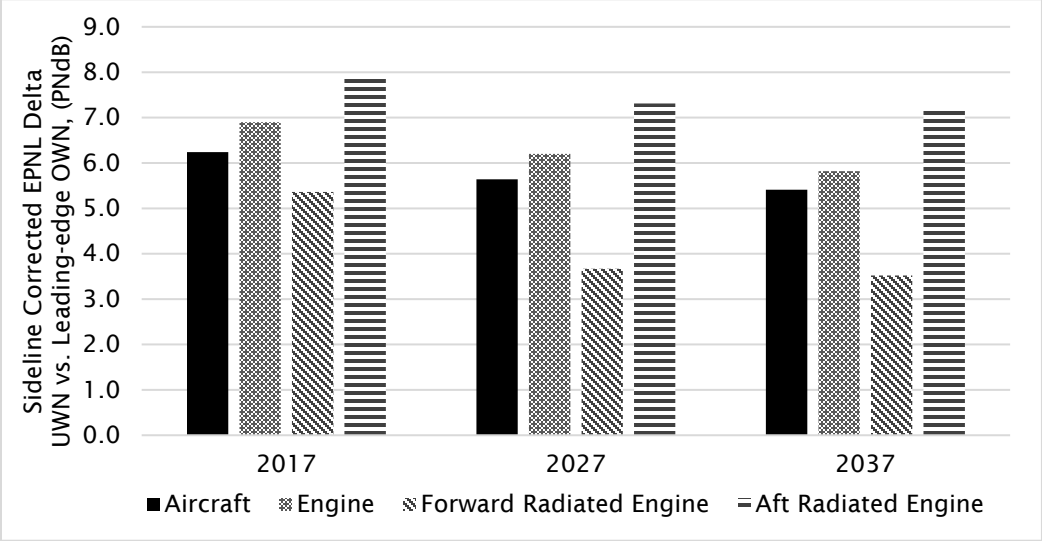

Figure 21. Preliminary (pre-optimization) sideline noise comparison of UWN and leading-edge-mounted OWN configurations under different technology assumptions.

Five-level full factorial and 100-case Latin-hypercube designs of experiments are combined into a single design of experiments to thoroughly sample the nacelle location design space within ANOPP. The ANOPP noise responses are fit to the nacelle location parameters using a single layer artificial neural network (ANN) with hyperbolic tangent nodes (see surrogate profiler plots in Figure 22), resulting in a root mean square EPNdB error of less than 0.105.

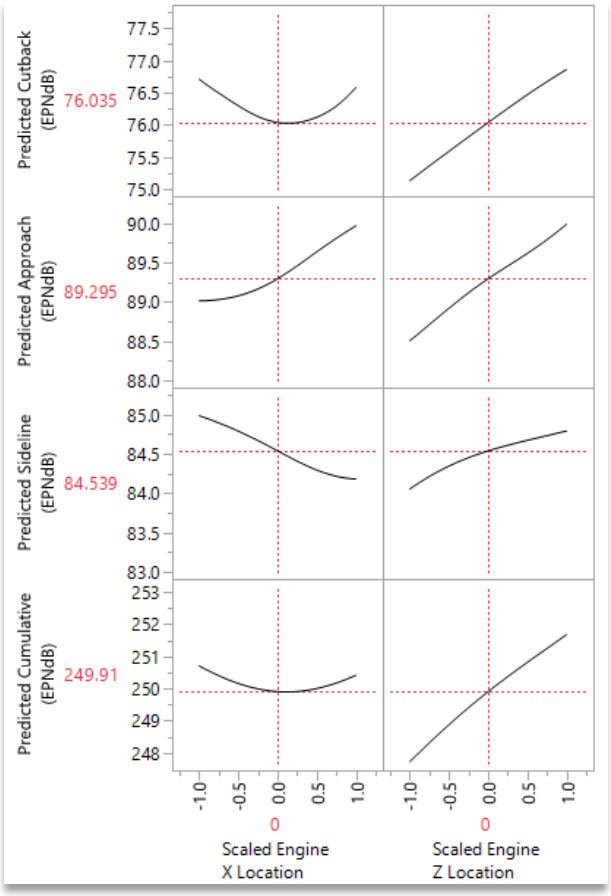

Figure 22. Example view of ANOPP surrogate model.

Milestone(s)
Initial ANOPP noise analysis was performed.

Major Accomplishments
ANNs were fit to the approach, cutback, sideline, and cumulative forward mounted OWN and UWN noise responses as a function of the nacelle location parameters. This directly supported generating data to select nacelle location in Task 5.

Publications
None

Outreach Efforts
None

Awards
None

Student Involvement
Andrew Burrell (Ph.D. student at the time) ran ANOPP and fit surrogate models to the noise responses.

Task 7 – Stage 2 Design: Engine Re-design and Airframe Re-optimization (Forward Mounted OWN)

Objectives

The following working MDAO problem statement was adopted:

- **Minimize**: fuel burn for a baseline mission
- **Subject to**: range and detailed side constraints
- **With respect to**: design variables including engine nacelle position (focusing on forward placement), nacelle and wing geometry, engine cycle, and operating condition
- **Given**: baseline single-aisle aircraft model and mission profile
- **Returning**: fuel burn

This task continues previous work with a higher bypass/larger diameter engine to potentially exploit the additional clearance above the wings.

Research Approach

The stage 2 optimization approach is identical to the stage 1 approach and will not be repeated here. We describe details of the process in (Ahuja, et al. 2023). However, we made new assumptions and redesigned the engine cycle. These assumptions are described here.

The bypass ratio can potentially improve the propulsive efficiency of an engine. This can be achieved by re-designing both the core and the fan, although the former is a significantly more expensive endeavor than the latter. Engine manufacturers typically do not design new cores for a single aircraft unless there is a significant market demand and financial incentive to do so. As such, assuming the OWN configuration were to come out within the next 10 years, the most viable option is to use a commercial off-the-shelf (COTS) engine that has the necessary thrust for the vehicle. The OWN configuration we investigate is similar in size to the A320neo and as far as current commercial off-the-shelf engines are concerned, the PW1100 Geared Turbofan engines are likely candidates for this vehicle.

However, one of the biggest advantages of the OWN configuration is the ability to integrate higher bypass ratio engines above the wing as ground clearance constraints for the nacelle are not a factor. However, if the PW1100 GTF series engines represents the best state of the art engine for this class of airframe and a new engine development program is not financially feasible, a middle ground could be a re-fan of the engine, which would be substantially cheaper than designing a new engine from scratch.

In this process, the engine core is fixed, but the components on the low-speed spool i.e. the low-pressure compressor and the fan are allowed to change. Thus, an increase in bypass ratio is achieved by decreasing the fan pressure ratio (allowing the low-pressure compressor pressure ratio to change accordingly), which results in a larger fan diameter. Thus, more airflow passes through the fan/bypass duct rather than the core, which increases bypass ratio and thus propulsive efficiency. The power produced by the fixed core, however, limits how much the fan can grow and thus there is a limit to the bypass ratio that can be achieved with this approach. Other limitations come from the aerodynamic performance of a larger nacelle and its detrimental impact on drag. At some point, the drag penalty from a larger nacelle overcomes the fuel benefit from a higher bypass ratio engine, limiting the feasible growth of the fan. Whether the core mechanical power constraint or the aerodynamic penalty constraint is hit first depends on the engine core design and the aerodynamic characteristics of the airframe, so it is problem dependent.

The baseline engine selected for this project is a notional PW1133 geared turbofan currently found on the A321neo models. A derated version of this engine is also found on the A320neo, a 150-pax class vehicle which the OWN and UWN configurations studied here were scaled to. This notional model of the engine was developed in EDS using publicly available data such as from the ICAO Emissions Databank and the EASA Type Certificate Data Sheet.

FLOPS-NPSS-WATE++ models of the OWN and UWN configurations were developed to get initial estimates of the block fuel burn for each case. Then, the fan pressure ratio was decreased from the baseline value of 1.52, keeping a fixed core, and the block fuel burn for each configuration was tracked. Note, that the weight impacts of a larger fan were tracked through WATE++, and FLOPS empirical wetted area/form factor estimates for nacelle drag were used to monitor the drag penalty of

the larger nacelle. The plots below show the block fuel vs FPR trend for OWN and UWN as well as the fan diameter variation with FPR.

From the monotonic trends in block fuel burn in Figure 23 (ignoring the FPR 1.5 case as a likely numerical convergence anomaly), it is apparent that the improved propulsive efficiency from a larger fan is the driving force behind the fuel burn reductions, given our modeling assumptions. It should be noted that NPSS consistently failed to converge for any FPR lower than 1.4, suggesting that this notional PW1133 core cannot power a larger fan.

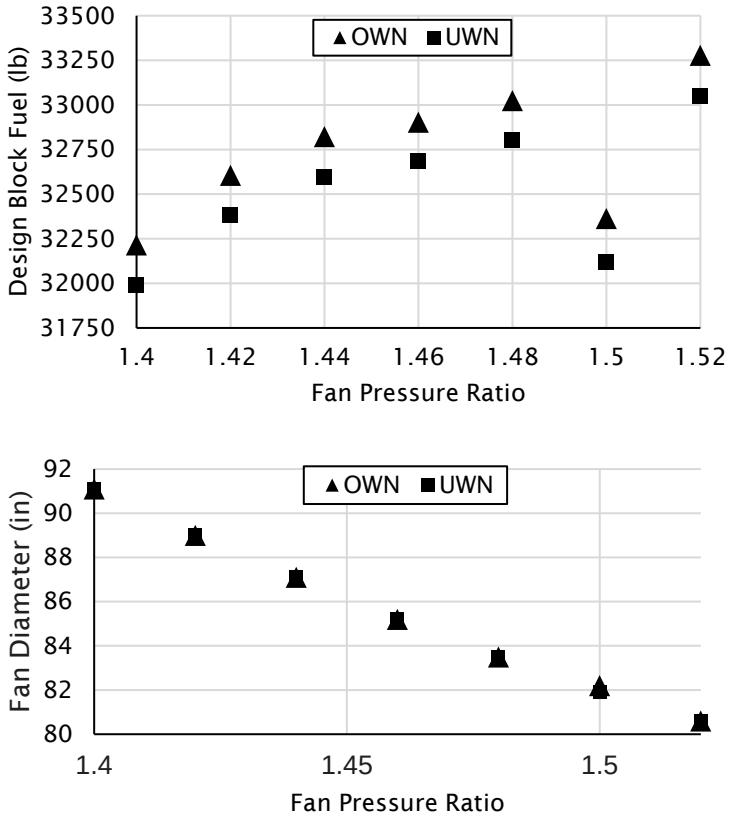

Figure 23. Design block fuel depends on fan pressure ratio, which in turn depends on fan diameter.

The results above show that a FPR of 1.4 will produce the lowest block fuel burn for both OWN and UWN, however, only the OWN can accommodate the larger fan. The UWN concept has ground clearance constraints that limit how much the fan can grow. To determine the smallest allowable FPR for the UWN that does not violate ground clearance constraints, we first looked at the airport planning manual for the A320neo aircraft featuring the derated PW1133 engine. The minimum ground clearance for this configuration is 18 inches. When comparing the A320neo to the A320-200 (older) variant, it is apparent that Airbus was able to fit a new engine on the same airframe with minimal changes but required a 4-inch reduction in minimum ground clearance. The 737-8 on the other hand makes more significant changes to the 737-800 airframe to accommodate the larger engines and takes a 1–2-inch reduction in minimum ground clearance.

Assuming we cannot reduce minimum ground clearance below 17 inches, to mount a larger fan for the UWN, we would need some combination of the following options:

- Mount the nacelle closer to the wing like The Boeing Company did with the 737-8, which would have aerodynamics implications,
- Incorporate a longer landing gear, but that would have weight penalties,
- Change the wing dihedral, which would have stability constraints, or

- Use thinner nacelles.

To avoid major airframe re-design, a fan diameter increase of 3 inches for UWN could be accommodated by mounting the engine further up with a thinner nacelle without going below 17-inch minimum clearance. This corresponds to an FPR of 1.48. For OWN, to maintain the same clearance between the wing and nacelle as in 2022 work, we moved the nacelle farther above the wing by about 9 inches.

We repeated the optimization procedure of stage 1 for with these assumptions. There was a surprising result: when the optimized shapes from stage 1 were simply adjusted for different engine diameters and nacelle position, these adapted stage 1 optimum shapes performed better than the stage 2 optimized results. The OWN had a fuel flow rate of 2362 lb/h at 40,000 ft, Mach 0.8, while the UWN had 2241 lb/h; the OWN fuel flow rate is 5.4% higher. There are many possible explanations, including a less effective geometry parameterization through an active subspace dimensionality reduction technique (Mufti, et al. 2022).

Milestone(s)
Optimization of OWN and UWN with larger engines was completed.

Major Accomplishments
Optimization and comparison of OWN and UWN designs was completed under cruise conditions for engines with larger bypass ratios.

Publications
None.

Outreach Efforts
None.

Awards
None.

Student Involvement
None.

Task 8 – Stage 3 Design: Nacelle and Wing Optimization (Aft Mounted OWN)

Objectives

The following working MDAO problem statement was adopted:

- Minimize: fuel burn for a baseline mission
- Subject to: range and detailed side constraints
- With respect to: design variables including engine nacelle position (focusing on aft placement), nacelle and wing geometry, engine cycle, and operating condition
- Given: baseline single-aisle aircraft model and mission profile
- Returning: fuel burn

This task continues stage 1 work using the same engine and airframe models, except aft-mounted engine locations are considered rather than forward-mounted locations.

Research Approach

The stage 3 optimization approach is identical to the stage 1 approach, described in (Ahuja, et al. 2023). The engine and airframe models are also identical to those used in Stage 1. The only difference between stage 1 and 3 is the location of the nacelle.

Like in stage 1, we first conducted a nacelle placement study and picked a baseline location for optimization semi-arbitrarily as shown in Figure 24. The results from this study showed that like for the forward mounted OWN configuration, moving the nacelle farther away from the wing is better for performance, as seen in Figure 25. As such, we picked a baseline TE location that was roughly as far away from the wing as the OWN LE case in Stage 1.

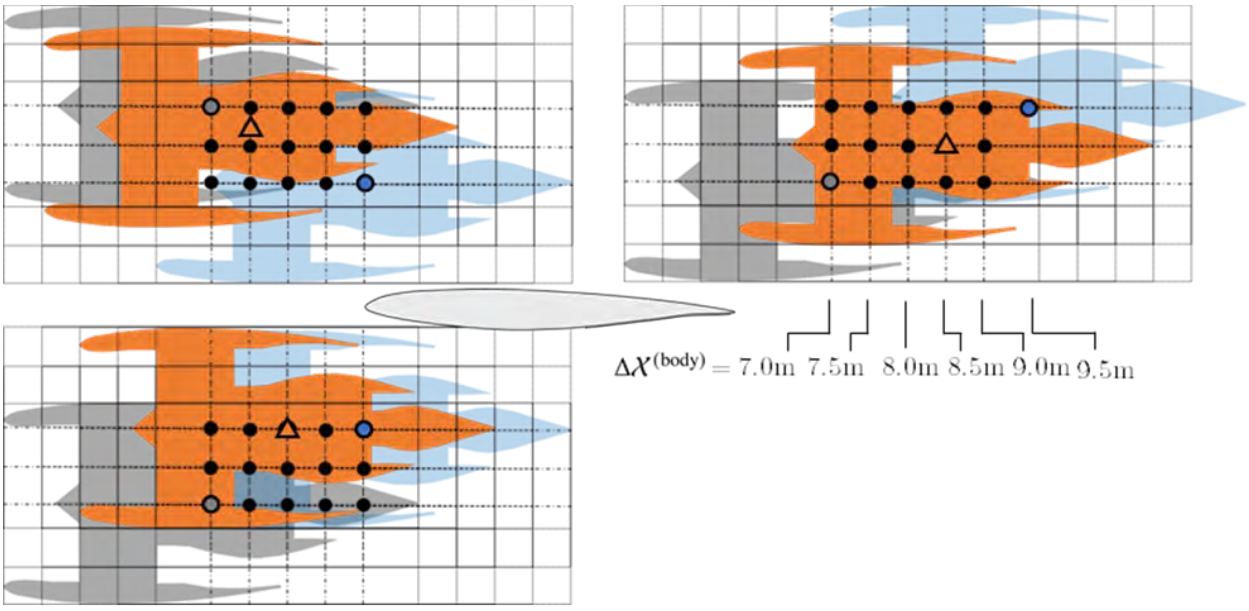

Figure 24. Orange locations are final selections for OWN and UWN.

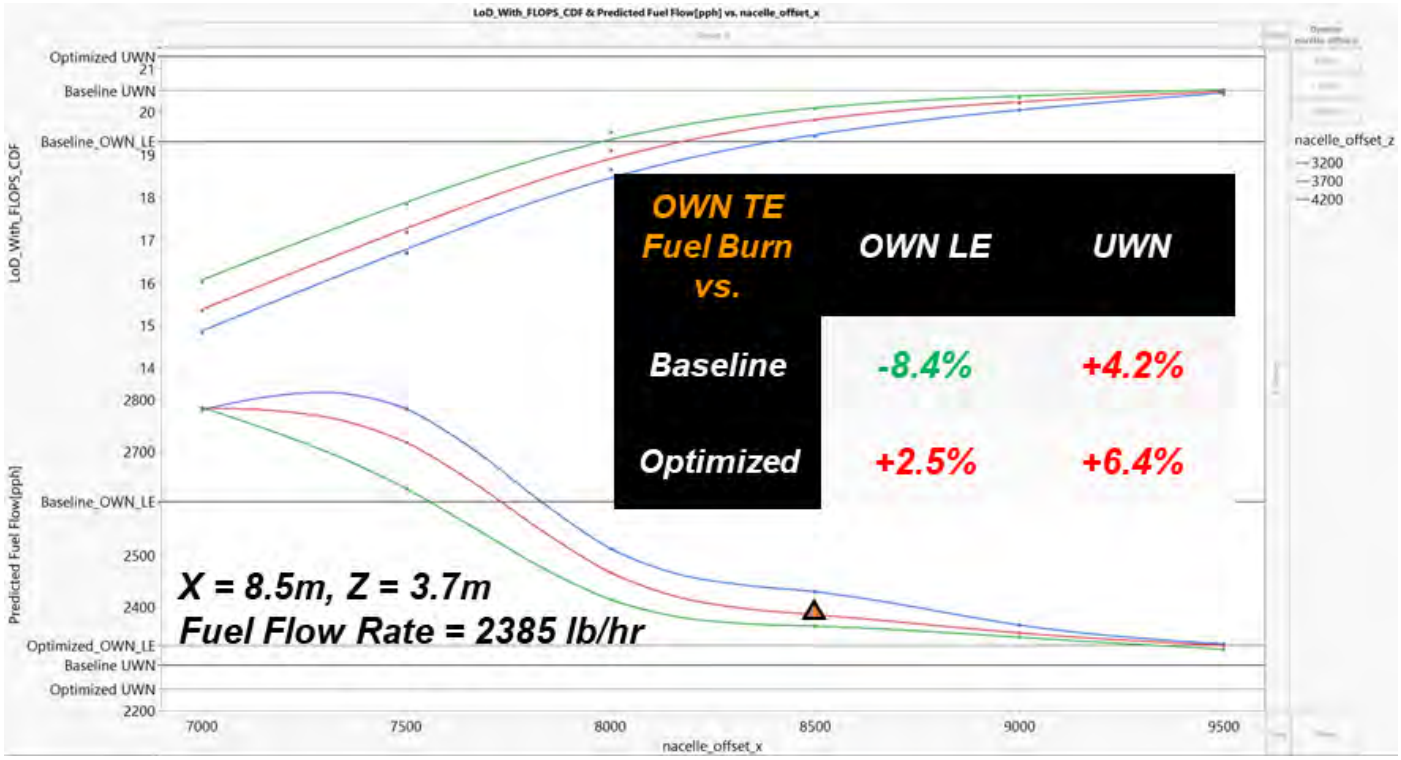

Figure 25. *L/D* and fuel flow trends with aft nacelle location with the chosen location's baseline performance highlighted

We repeated the optimization procedure of stage 1 for with these assumptions. The results of the optimized configuration are compared to the UWN and OWN LE configurations in Figure 26. We see that even though the baseline OWN TE configuration outperforms the baseline OWN LE case, the improvement in performance is much smaller. Thus, the optimized OWN TE case has a roughly 5% higher cruise fuel flow rate than the optimized UWN as opposed to 4% for the OWN LE case.

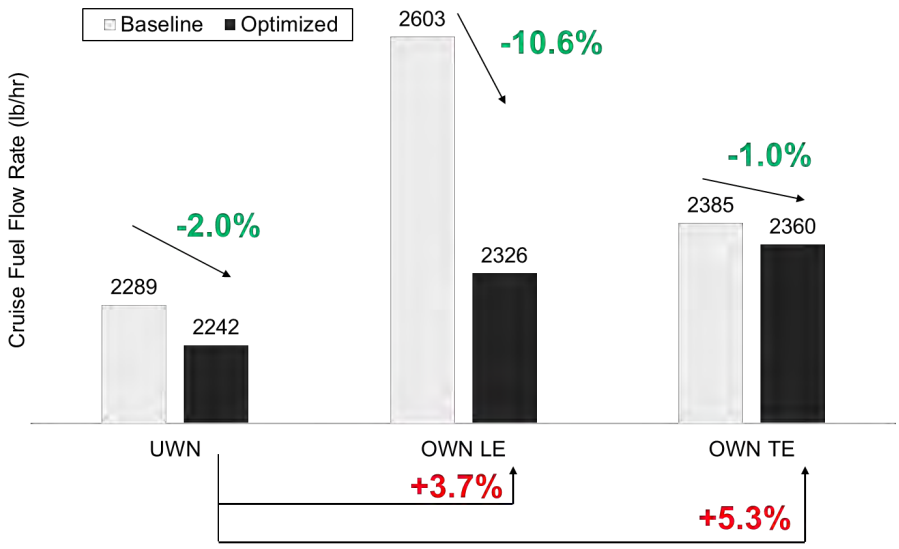

Figure 26. Comparison of the optimized OWN TE configuration cruise fuel flow rate to the OWN LE and UWN configurations.

Milestone(s)
OWN TE configuration optimization was completed.

Major Accomplishments
Completed optimization and comparison of OWN and UWN designs under cruise conditions for forward and aft mounted locations.

Publications
None.

Outreach Efforts
None.

Awards
None.

Student Involvement
None.

Task 9 - Mission Analysis and Trajectory Optimization Setup

Objectives

In a separate task, we performed CFD-based aero-propulsion optimization for cruise conditions. We then aimed to evaluate fuel burn for OWN and UWN configurations over a mission including other mission phases such as climb and descent. Since 2022 (see ASCENT A50 2022 annual report), we reoriented our objective to delve into a more fundamental reformulation of aero-propulsion-mission analysis.

Research Approach

The mission analysis task has diverged substantially from what we envisioned at the beginning of this research in 2020. Georgia Tech had previously relied heavily on its Environmental Design Space suite of mission sizing and synthesis tools built around NASA's FLOPS mission analysis and the propulsion cycle analysis based on NASA's Numerical Propulsion System Simulation (NPSS). During our research, we learned that our aero-propulsion integration physics required fundamental changes to mission analysis assumptions. This problem arose because almost all existing conceptual mission analysis codes assume relative independence between airframe aerodynamic drag polars and propulsion cycle (see ASCENT A50 2022 annual report for more information). Such assumptions may be highly inaccurate if there is tight coupling of aero-propulsion physics in novel concepts such as those for OWN or boundary layer ingesting aircraft. Our preliminary tests suggested that fuel burn errors due to traditional mission analysis tools may be comparable or even larger than the difference between OWN and UWN results. At about the same time in 2022, we had very fruitful discussions with NASA experts who were working in a similar area. In consultation with our FAA project manager, we directed our effort toward developing novel mission analysis methods and code. In 2023, we completed mission analysis to allow comparison of OWN and UWN optimum configurations in Task 1.

The mission analysis method which produced the results presented here is based on a what is broadly known as *trajectory optimization* (Kelly 2017), which is a process for finding the state values (e.g., position, velocity) across the trajectory (e.g., time history) which are somehow dependent on a set of control variables and produce a value in some objective function, which is a function of the entire trajectory, in general. The optimizer seeks to optimize the objective function with respect to these control variables and the system's resulting states, subject to the governing equations of the problem (referred to in this context as "equations of motion" or as the system's "dynamics model").

We used a two degree-of-freedom (2-DoF) dynamics model (Equation 1) based on Newton's Second Law (Chakraborty and Mishra 2021) ignoring the earth's curvature and rotation (Anderson 1999) avoiding an energy-based climb and descent optimization used in FLOPS and similar codes (Capristan and Welstead 2018). The details of the model are given in the 2022 Annual Report. We built the trajectory optimization with NASA's Dymos optimal control library (Falck, et al. 2021) for NASA's OpenMDAO framework (Gray, et al. 2019).

$$\dot{V} = \frac{F_{w,z}}{m} - g\sin(\gamma)$$
$$\dot{\gamma} = \frac{1}{V}\left[\frac{F_{w,z}}{m} + g\cos(\gamma)\right]$$

V	Tangential velocity magnitude
$\dot{V}$	Time rate of change of velocity magnitude (tangential acceleration)
$F_{w,x}$	Force applied (not due to gravity) in wind axis system parallel to velocity
$F_{w,z}$	Force applied (not due to gravity) in wind axis system perpendicular to velocity in vertical plane
γ	Flight path angle between velocity vector and horizontal datum (flat earth assumed)
$\dot{\gamma}$	Time rate of change of flight path angle
m	Mass of vehicle
g	gravitational acceleration (assumed constant)

Equation 1. Equations of motion governing 2-DoF mission analysis

During the first half of 2023, we began a series of developmental experiments to compare mission fuel burn under different physics modeling assumptions. While originally it was planned to develop at least three distinct iterations of the mission analysis, not all three were implemented fully within the span of the project.

The first of the three iterations of the mission analysis, as noted above, used direct reading or surrogate modeling of FLOPS disciplinary analyses results, but ran the trajectory optimization in a different program, the Dymos optimal control library in the OpenMDAO framework from NASA. In one test, we used identical aerodynamics polars, engine model ("engine deck"), and the weights model from FLOPS results while using the newer equations of motion formulation (Equation 1). In this test, we found on the order of 1% fuel burn discrepancy is attributable to the equations of motion alone. Other discrepancies on the order of 1% are attributable to different assumptions about regulatory requirements in descent, for example. with mission phase constraints representative of real operational constraints (e.g., maximum speed of 250 kn below 10,000 ft altitude, as required by FAR-91.117 (United States Department of Transportation, Federal Aviation Administration 2024).

The second of these iterations was intended to replace the imported FLOPS results with custom in-the-loop implementations of FLOPS disciplinary (e.g. weights, aerodynamics, propulsion) methods within the analysis code (termed "Olympus" by the development team) to attempt to reproduce these results with only the input data used by FLOPS. Some routines were implemented by referring to published literature (Wells, Horvath and McCullers 2017). Others were implemented by referring directly to the FLOPS 8 source code and FLOPS 8 and FLOPS 9 documentation. As an aside, the Aviary analysis code by NASA (Aretskin-Hariton, et al. 2024, Gratz, Jasa and Kirk 2023), released in December 2023, implements these methods as well. This intermediate, second iteration was run in a semi-complete form, but the mission analysis of the OWN aircraft never converged in this iteration. Due to time constraints, and a focus on testing, this was prematurely put on hold to pursue final mission analysis results integrating the high-fidelity aero-propulsive surrogates from CFD analysis. Attempts to replace direct execution of the EDET methods with surrogate models of the EDET results were unsuccessful, due to unresolved errors in the partial derivatives (Jacobian) computation.

The third and final iteration of mission analysis development for this project incorporated artificial neural network aero-propulsive surrogates based on the OWN and UWN forward-mounted optimized nacelle and airframe geometries from earlier stages of the project. These were used in the mission analysis, replacing the propulsion and aerodynamics methods and results previously read from FLOPS output. The "final" results reported for this project were produced in this iteration, which is deemed the most accurate iteration of the mission analysis development as it accounts for the coupled aero-propulsion interactions inherent in the OWN configuration, not captured by the FLOPS analysis.

By running the third iteration mission trajectory optimization codes for the UWN and OWN 150-pax configurations, state timeseries (Figure 29) were produced for the OWN and UWN vehicles. These trajectories include only the central, in-flight portion, beginning with climb, of the specified design mission (Figure 27-Figure 31). Reserve mission trajectories were developed earlier in the design process but are not presented here in the results.

The results for these trajectories are consistent with the prediction of higher fuel burn with OWN than UWN, as indicated by the lower final gross weight for OWN compared to UWN shown in Figure 27 and Figure 31. A reference case was run in the FLOPS tool with the same sizing parameters as used in the 2-DoF analysis, and that data is plotted in these figures as well. The problem formulation and optimization methods are slightly different between these tools. FLOPS may minimize the fuel burned or time elapsed during only the climb segment, or maximize the *L/D* ratio for the descent (Capristan and Welstead 2018), while the 2-DoF approach presented here wholistically optimizes the fuel burn *over the entire mission*, and no distinction is made in the objective for different phases.

The free variables the optimizer adjusts to optimize the mission fuel burn are the normalized tangential control mapped to an engine control and the normalized vertical control parameter which is mapped to angle of attack α in this process. These are inputs, along with the altitude and Mach number, to the aero-propulsion surrogates used to predict the coupled aerodynamic force coefficients and the engine fuel burn rate.

The states which the optimizer adjusts in pursuit of physical consistency with the controls throughout the mission are the altitude, distance traveled over the ground, speed (assuming no wind), flight path angle, and the gross weight of the aircraft. All but the latter define the position and velocity of the point-mass aircraft model in the mission, and the latter is related to the thrust via the fuel burn rate of the propulsion system, assuming that fuel burn is the sole source of change in weight. These are plotted, directly or indirectly (in the case of flight path angle, the speed and flight path angle are used to find the climb rate) in Figure 28 in terms of distance and in Figure 29 in terms of time (which may be considered another state, but

one which is independent of all others). A typical presentation of an aircraft's operating envelope may use a "sky map" such as the one plotted in Figure 30 for the trajectory of each configuration. In this figure, most of the flight is spent at or near the upper right corner where the aircraft cruises at a relatively high Mach number and altitude. To highlight the difference in the final converged trajectory based on the 2-DoF equations of motion and the mission-level objective function versus the legacy FLOPS mission analysis optimization routines, the climb and descent phases are highlighted in Figure 31. Note that the 2-DoF Olympus program attempts something resembling a "step climb" (Figure 28, Figure 29, and Figure 31) where it begins to plateau in altitude and velocity partway between 20,000 and 30,000 ft altitude, finding an apparently more optimal path than what FLOPS follows.

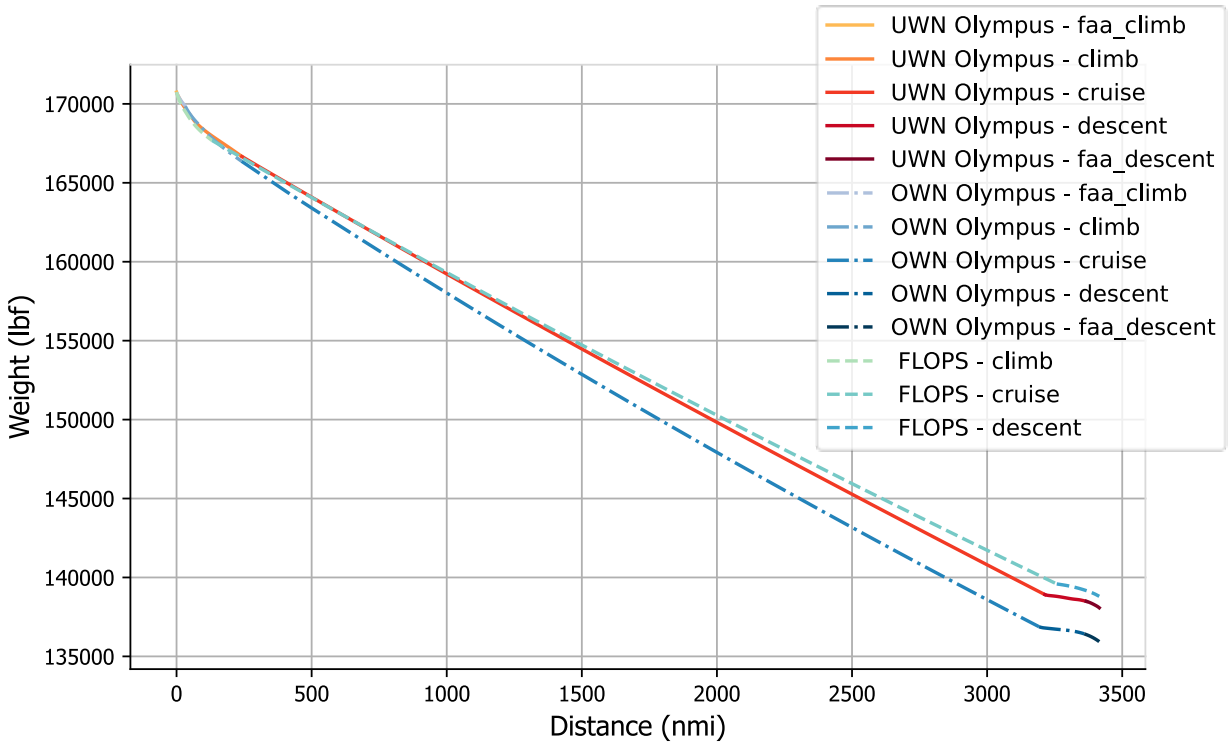

Figure 27. Gross weight versus distance for different configurations' mission analyses.

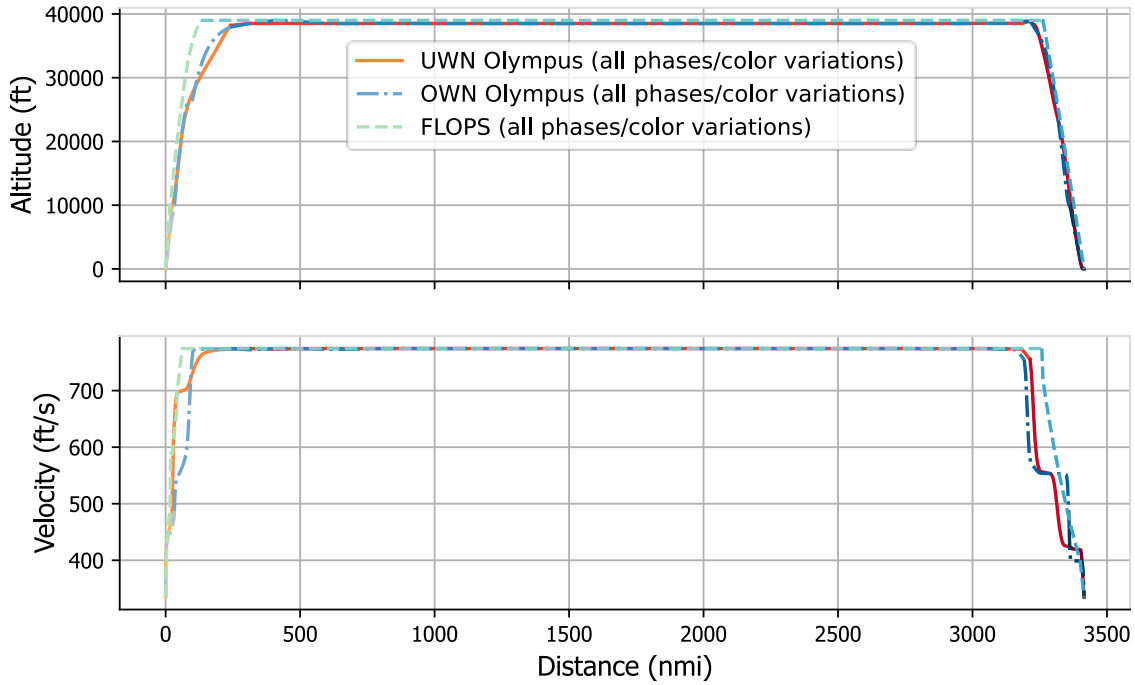

Figure 28. Flight conditions vs distance over the ground for different configurations' optimized trajectories, lighter colors appearing earlier in the mission than darker colors.

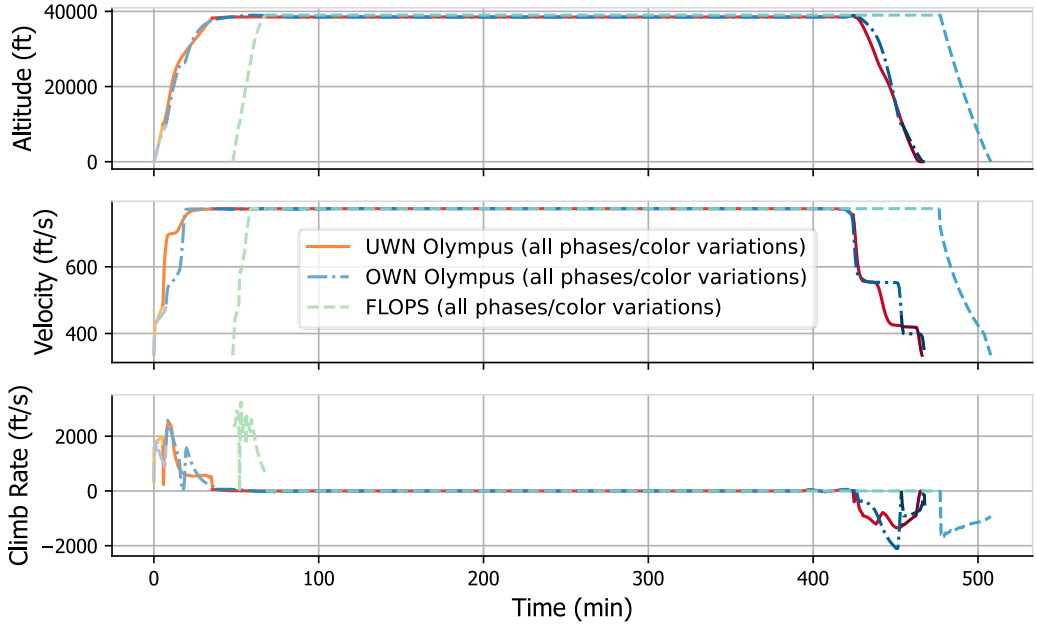

Figure 29. Design mission timeseries optimized (for minimum fuel burn via maximum final weight) for OWN and UWN configurations using 2-DoF ("Olympus") mission analysis code, with FLOPS' discontinuity (bottom plot) in climb rate at transition from climb to steady cruise.

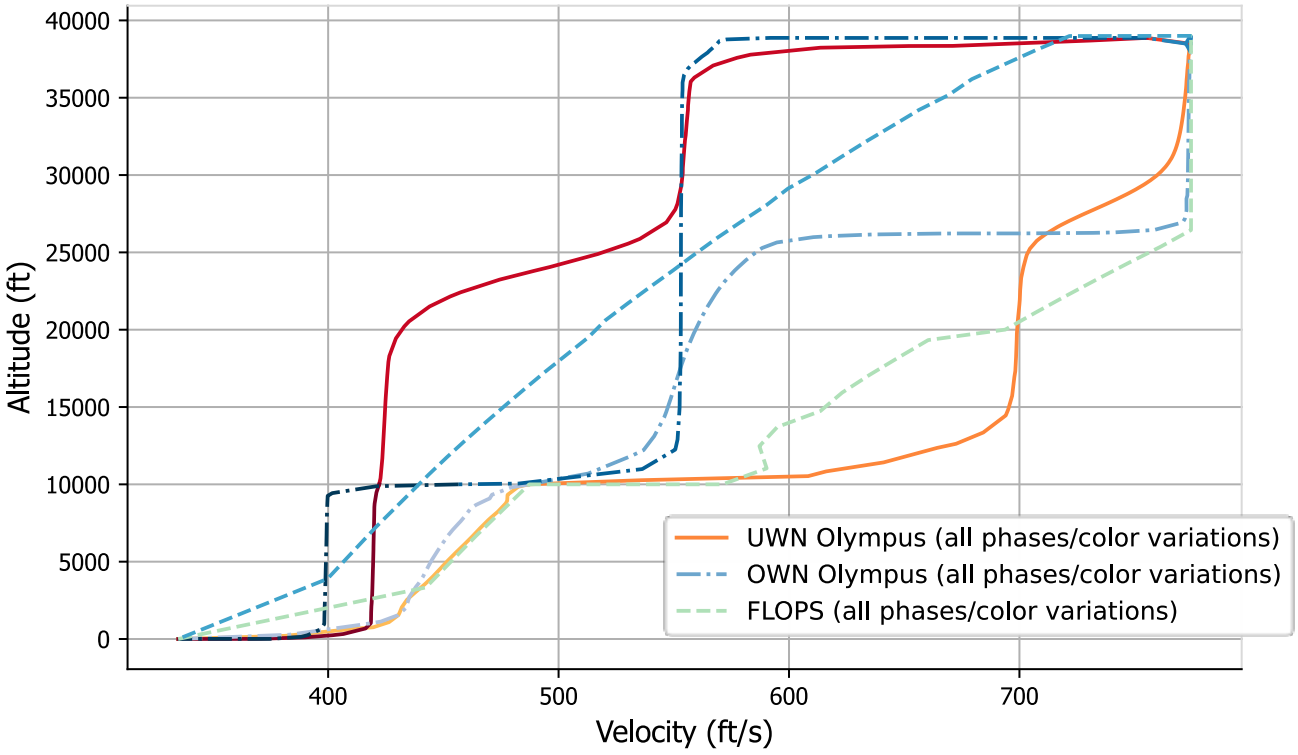

Figure 30. "Sky map" of flight condition history for each vehicle's optimized flight trajectory.

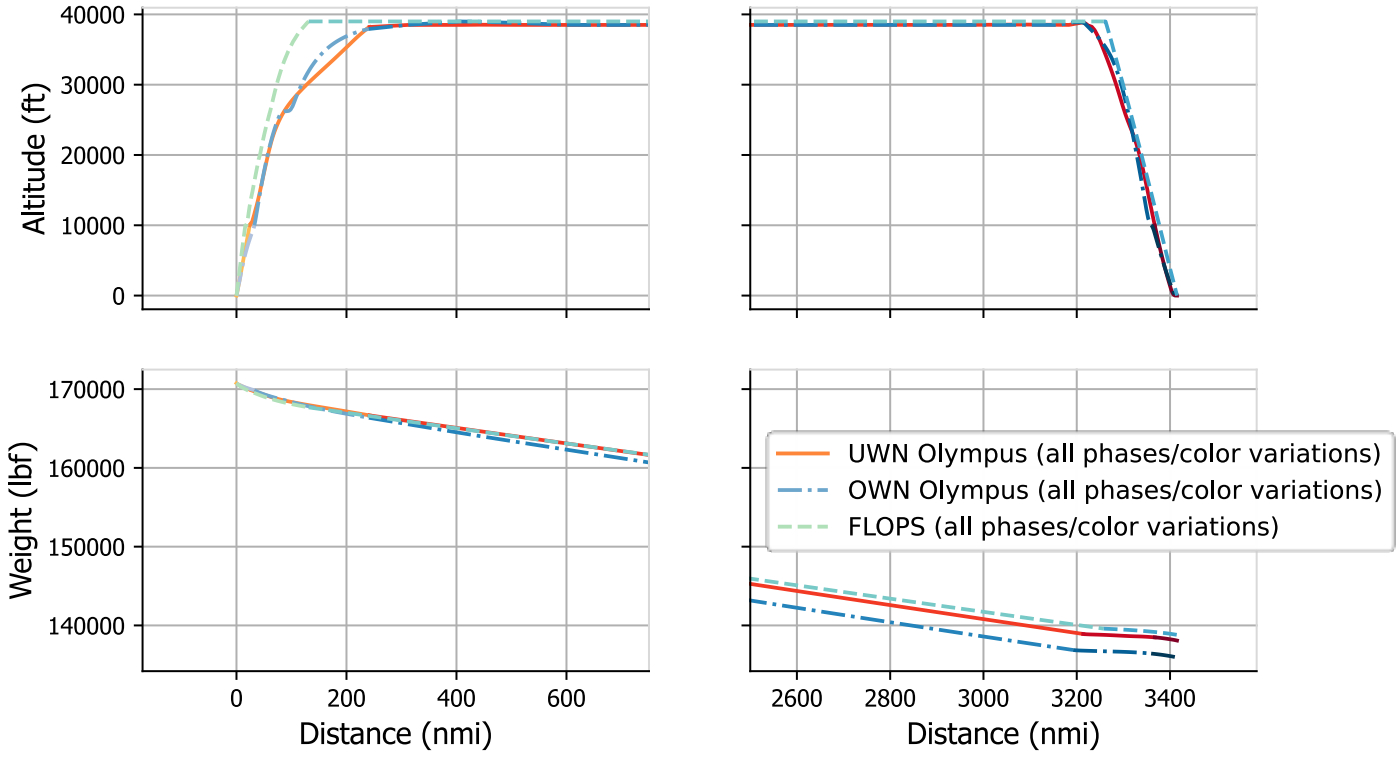

Figure 31. Close-up of mission end phases — climb and descent — for each trajectory

Convergence of the trajectories were non-trivial to achieve, once the models were built and the aero-propulsion surrogates integrated, requiring extensive adjustment optimizer settings and trial-and-error. The “final” results presented here likely depend on those optimizer settings, among other variables. The settings used for the IPOPT optimizer which converged the final trajectories shown here are given in Table 6.

Table 6. Optimizer settings used for final trajectory optimization (OWN and UWN)

Setting	Value
acceptable_tol	1e-06
alpha_for_y	safer-min-dual-infeas
compl_inf_tol	1e-05
constr_viol_tol	1e-05
file_print_level	5
hessian_approximation	limited-memory
linear_solver	mumps
max_iter	1500
mu_init	0.1
mu_strategy	adaptive
nlp_scaling_method	gradient-based
print_level	0
print_user_options	yes
sb	yes
tol	1

The mission-level fuel burn and comparison between the results for each configuration are shown in Table 7. First, the endpoint total (gross) weights (starting at climb, ending at the end of descent) are shown for each of the vehicle missions modeled using the 2-DoF analysis code written for this study. It shows the difference in these as the fuel burn (the only accounted change in weight), and the percent changes between the configurations relative to the configuration named in the column header (first relative to the FLOPS analysis, then relative to the UWN 2-DoF analysis). It can be seen from this that the final difference between the UWN and OWN configurations (according to the 2-DoF analysis) was a 7% higher fuel burn for the UWN configuration compared to the OWN configuration.

Table 7. Summary results for mission optimization for fuel burn for OWN, UWN, and FLOPS.

	Start [lbf]	Final [lbf]	Fuel Weight [lbf]	% Diff (OWN FLOPS)	% Diff (UWN Oly)
OWN FLOPS	170740	138805	31935	0%	-2%
UWN Olympus	170740	138079	32661	2%	0%
OWN Olympus	170740	135934	34806	9%	7%

No “simulation” (time-stepping numerical integration) based on the equations of motion in any of the development iterations was successful. The researchers conjectured it might be due to the handling of discrete variables (number of engines, for example) in the OpenMDAO framework, which seems to have limited support for discrete variables in gradient-based optimization problems (The OpenMDAO Development Team 2022). The implication of this is that the final, converged, “optimal” trajectory may very well be physically inaccurate in terms of the precise states and state rates it predicts at points in time along the mission. A simple example of this phenomenon is shown in the documentation example for a simple, canonical mass-spring-damper problem (The Dymos Development Team 2022).

Milestone(s)

A comparison was conducted of 2-DoF vs. FLOPS mission fuel burn, controlling for aerodynamics, weights, and propulsion disciplines. Trajectory optimization was completed after OWN and UWN configurations were optimized in Task 7.

Major Accomplishments

A more general drag-free, thrust-free mission and trajectory analysis method was developed. An initial implementation was done in OpenMDAO and Dymos software.

Publications
None.

Outreach Efforts
Researchers met and collaborated with the NASA GASPy (predecessor of Aviary) and OpenMDAO development team.

Awards
None.

Student Involvement
Mengzhen Chen re-implemented some EDET aerodynamic methods from FLOPS for second-iteration Olympus development. Samuel Crawford implemented propulsion "engine deck" modeling/lookup functionality replicating FLOPS propulsion module's capability for first and second-iteration mission analysis and developed early mission analysis mimicking FLOPS mission analysis methods (replaced later by implementation in OpenMDAO framework). Samuel Moore and Savri Gandhi were PhD students at the time who contributed to the comparison of FLOPS with results from the framework implementing 2-DoF simulation, or development of scaffolding for debugging the mission analysis.

Task 10 – High Lift Physics Study

Objectives
By request from FAA stakeholders in 2022, we investigated a variety of physics phenomena and their potential impacts on high lift vehicle performance during takeoff. We focused on the aerodynamics of blowing or increased circulation. We optimized takeoff trajectories (for takeoff length) for both OWN and UWN configurations and investigated the effects of ground effect and an inoperative engine.

Research Approach
The high lift investigation was intended to be an opportunistic investigation of smaller scope than the other tasks. There was no shape optimization, and we used fixed designs for both OWN and UWN. To parallelize work alongside the previous tasks, we used the optimized designs from 2022 as starting points, as described in the 2022 Annual Report as well as our publication (Ahuja, et al. 2023). Those designs were optimized for cruise fuel burn and did not include flaps or slats. In this shorter effort, we did not optimize the flaps and slats but rather scaled and adapted geometries from the NASA High Lift Common Research Model (CRM-HL) as described in (Lacy and Clark 2020). Note that the present OWN vehicle is a 150-pax aircraft while the CRM is a larger 300-pax as shown in Figure 32.

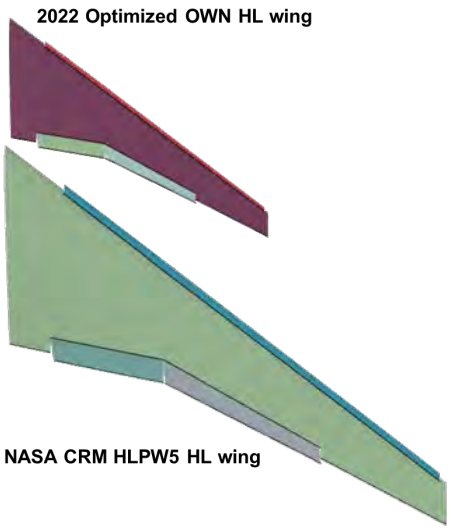

Figure 32. The slats and flaps configuration used in this study are based on the larger NASA CRM-HL.

For this effort, we did not design internal linkages or include detailed kinematic rules for the slats and flaps, though some flap geometry scripts were developed using Bezier curves. For another example of work on this area, see (Marfatia and Bergeson 2021). Rather, using the CRM-HL as a basis, we assumed two settings ("low" and "high") for high lift surface deflections. The low flap deflection is 10˚, and the high deflection is 25˚ as shown in Figure 33. The slat settings are tied to the flap deflection, and the slats are in a sealed position for the low deflection setting. We emphasize that these settings are not optimized.

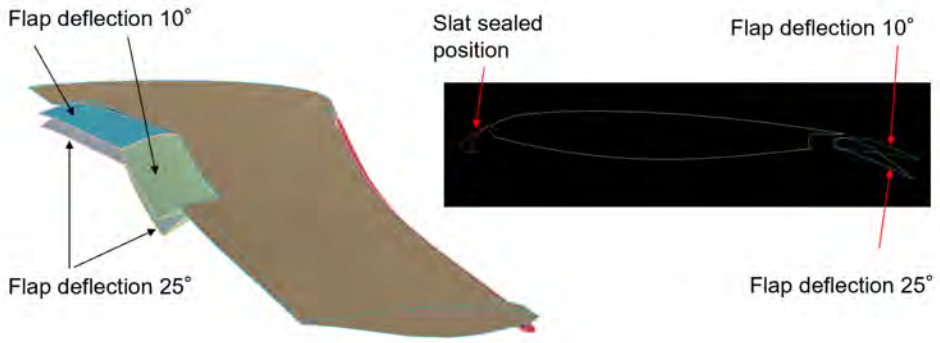

Figure 33. Two combinations of flap and slat settings are used in this study.

Example flowfields are shown for Mach = 0.2 and angle of attack α = 16˚ for both OWN and UWN with the two flap/slat settings. All cases use the same engine cycle model and power code of 50 (full throttle).

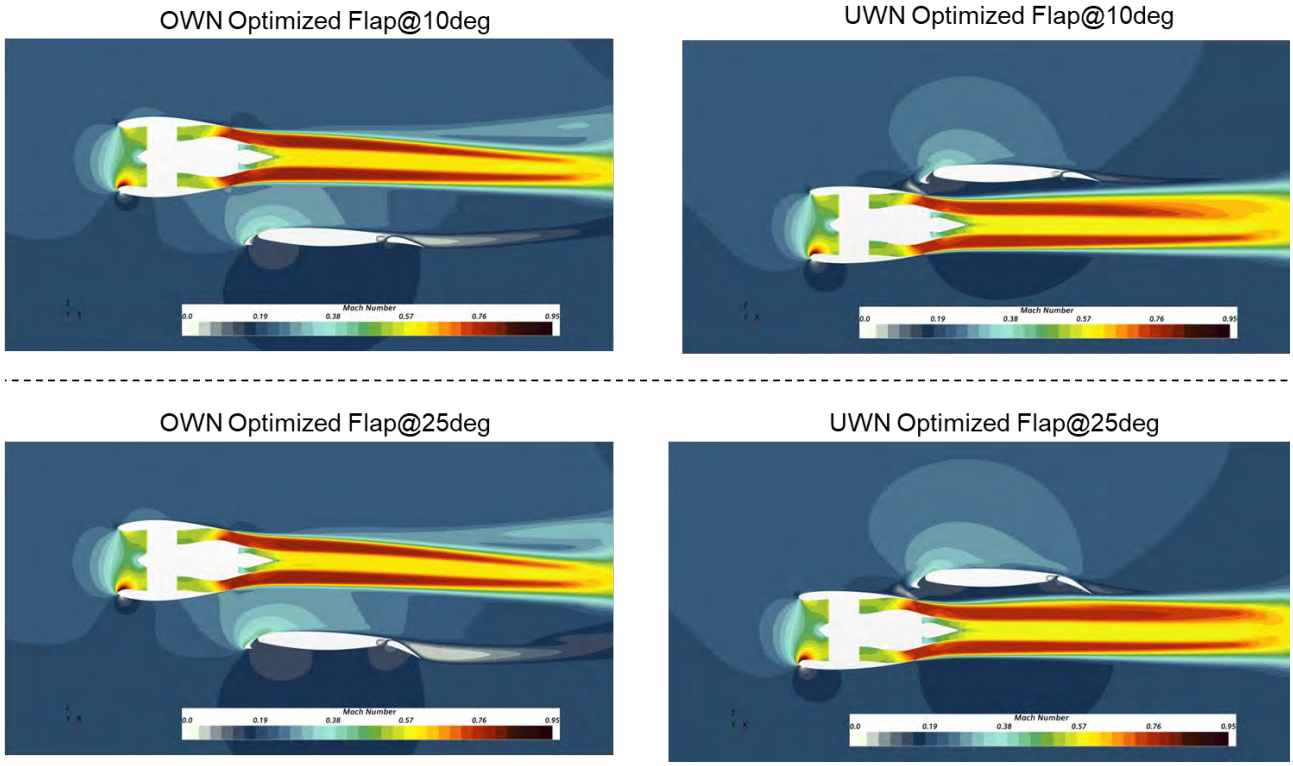

Figure 34. Example flowfields shown for OWN and UWN with two deflection settings at vehicle a = 16˚.

Example lift and drag polars are shown below in Figure 35. There appears to be a significant aerodynamic advantage for both lift and drag in this case.

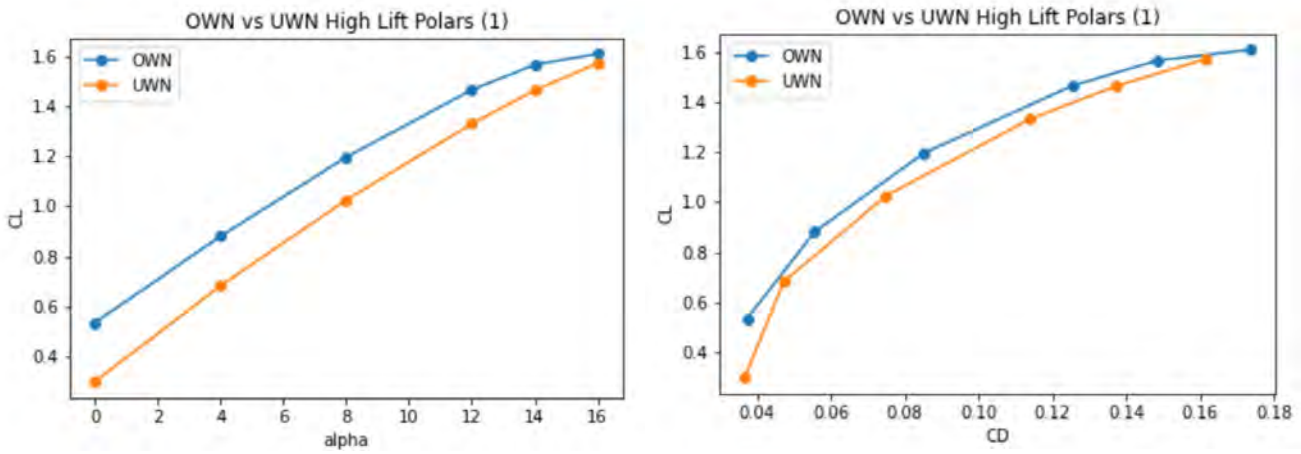

Figure 35. Example lift and drag polars with "low" settings for flaps and slats, Mach = 0.2, PC = 50.

We next accounted for ground effect during the takeoff ground roll and rotation. Figure 36 below shows an example flowfield with the ground modeled as an inviscid slip wall boundary condition. We assumed the location of rear landing gears and pivoted the aircraft about this location when performing a sweep over angle of attack.

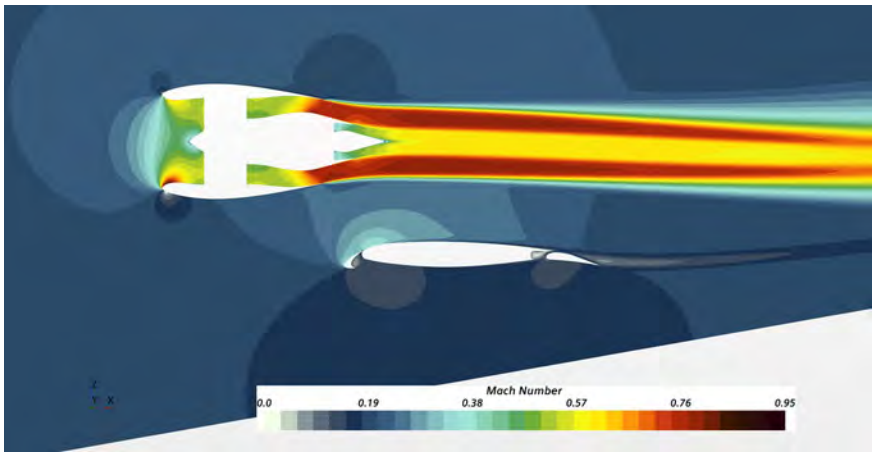

Figure 36. Ground effect modeled with an inviscid slip wall.

Figure 37 shows the pressure coefficients on the aircraft surface as well as the ground. Figure 38 shows a comparison of example lift polars for OWN and UWN with ground effect – there is again an aerodynamic advantage for OWN.

Figure 37. Pressure coefficients shown for aircraft and ground for OWN (left) and UWN (right).

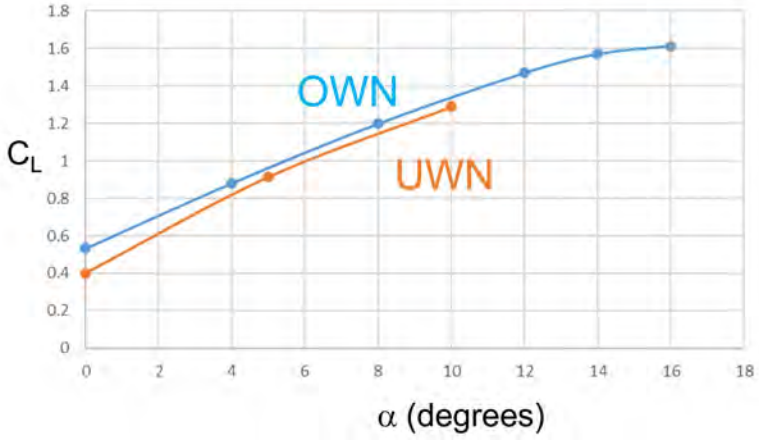

Figure 38. Example lift polars with ground effect showing potential OWN lift benefit (shown for "low" flap/slat settings).

Finally, we also studied the "one engine inoperative" (OEI) condition. FAR-25 requirements for OEI performance affect the calculation of balanced field length. However, there is no clear mapping to CFD boundary conditions. For example, we might implement impermeable wall boundary conditions for the nacelle such that the inoperative engine is essentially a bluff body. However, we judged this to be unrealistic because a malfunctioning engine is unlikely to instantly freeze or to completely stop mass flow. For a qualitative analysis, we used idle power settings of PC=21. In our preliminary analyses, we found that the aerodynamic performance was not significantly affected by this setting. We judged that the simplifying assumptions of our OEI CFD analysis were too crude such that they are likely within the uncertainty of other physical simplifications. For example, we did not account for yaw, sideslip, and control surface deflections accompanying the loss of one engine. In subsequent takeoff trajectory analyses, we simply treated the OEI condition as a loss of half of the available thrust.

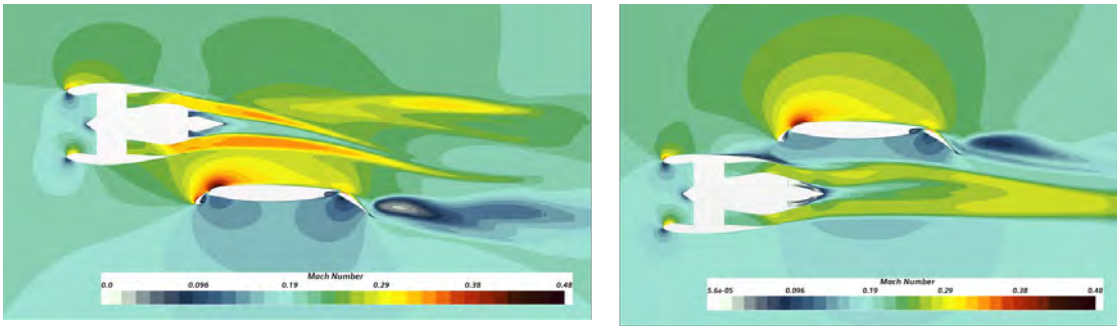

Mach = 0.2 , Altitude = 0 ft, alpha = 12°

Figure 39. Example flowfields shown for OEI condition.

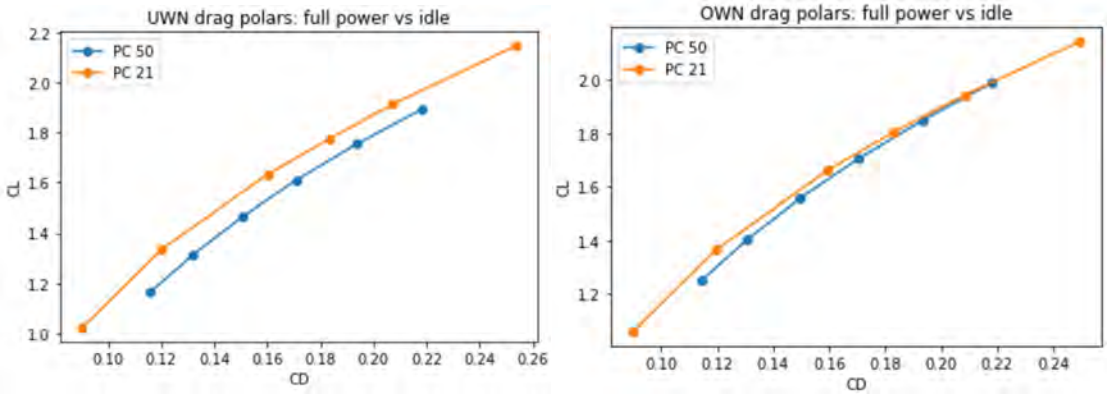

Figure 40. OEI modeled as idle power (PC=21). Note the lower aerodynamic penalty for OWN.

Finally, the above physics effects and aerodynamic polars were used to compare optimized takeoff field lengths for OWN and UWN vehicles. We used as a template an example OpenMDAO Dymos tutorial case for "Aircraft Balanced Field Length Calculation" (The Dymos Development Team 2022). We modified that aerodynamic polars to use quadratic response surface equations for the lift and drag polars and drag polars described previously. Preliminary findings for low flap/slat settings show an approximately 400 ft shorter takeoff field length for the OWN aircraft. Figure 41 shows an example result for balanced field length for the OWN. There is a bifurcation in the trajectory because the balanced field length (The Dymos Development Team 2022) must meet requirements for two scenarios: aborted takeoff and braking to a stop on the runway and takeoff with one engine inoperative and clearing an obstacle at the end of the runway. The OWN configuration has a balanced field length of about 5800 ft and the UWN requires 6200 ft.

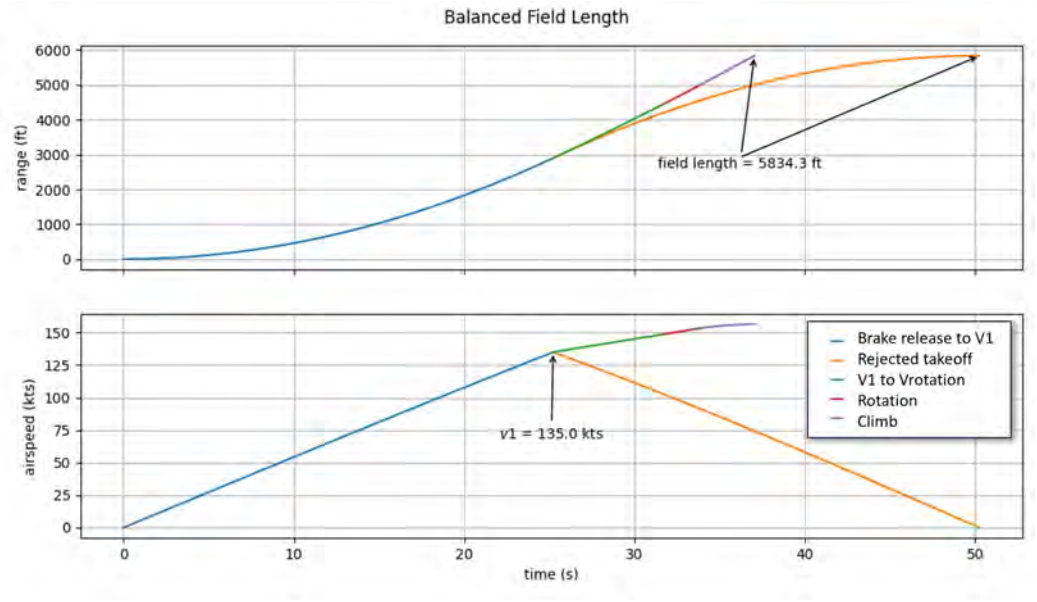

Figure 41. Example balanced field length calculation for OWN.

However, we presently judge that the 400 ft shorter field length for OWN is not significant enough to claim any major advantage. A complete redesign around the OWN configuration would potentially include different landing gear lengths/weights, different operations such as rotation angles, and different fuselage geometry to allow different rotation angles. Despite the apparent advantages in aerodynamic coefficients and takeoff field lengths in our simplified calculation, we can only make modest conclusions: there are no immediately obvious, qualitative "showstoppers" in OWN takeoff performance.

Milestone(s)
Automation scripts were created for high lift configurations. CFD polars were computed with ground effect as well as an OEI condition.

Major Accomplishments
Trajectory optimization for minimum takeoff length was completed using CFD polars in Dymos optimal controls software.

Publications
None.

Outreach Efforts
None.

Awards
None.

Student Involvement
Kavya Krishnan (PhD student at the time) contributed to high lift geometry preparation. Savri Ghandi (PhD student at the time) also supported this effort for some time.

References

Ahuja, Jai, Chung H. Lee, Christian Perron, and Dimitri N. Mavris. "Comparison of Overwing and Underwing Nacelle Aeropropulsion Optimization for Subsonic Transport Aircraft." *Journal of Aircraft* (American Institute of Aeronautics and Astronautics, Inc.), September 2023: 1–16.

Anderson, John D. *Aircraft Performance and Design.* McGraw-Hill Companies, Inc., 1999.

Aretskin-Hariton, Eliot, et al. "Multidisciplinary Optimization of a Transonic Truss-Braced Wing Aircraft using the Aviary Framework." *AIAA SCITECH 2024 Forum.* American Institute of Aeronautics and Astronautics, Inc., 2024.

Capristan, Francisco M., and Jason R. Welstead. "An Energy-Based Low-Order Approach for Mission Analysis of Air Vehicles in LEAPS." *AIAA Science and Technology Forum and Exposition.* Kissimmee: American Institute of Aeronautics and Astronautics, Inc., 2018.

Chakraborty, Imon, and Aashutosh Aman Mishra. "Generalized Energy-Based Flight Vehicle Sizing and Performance Analysis." *Journal of Aircraft* 58, no. 4 (2021): 762-780.

Constantine, Paul G. *Active Subspaces: Emerging Ideas for Dimension Reduction in Parameter Studies.* Philadelphia: SIAM, 2015.

Falck, Robert, Justin S. Gray, Kaushik Ponnapalli, and Ted Wright. "dymos: A Python package for optimal control of multidisciplinary systems." *Journal of Open Source Software* 6, no. 59 (2021): 2809.

Fujino, Michimasa, and Yuichi Kawamura. "Wave-Drag Characteristics of an Over-the-Wing Nacelle Business-Jet Configuration." *Journal of Aircraft* (American Institute of Aeronautics and Astronautics Inc.) 40, no. 6 (November 2003): 1177–1184.

Gautier, Raphaël, Piyush Pandita, Sayan Ghosh, and Dimitri Mavris. "A Fully Bayesian Gradient-Free Supervised Dimension Reduction Method Using Gaussian Processes." Edited by Habib N. Najm. *International Journal for Uncertainty Quantification* (Begell House, Inc.) 12, no. 2 (2022): 19–51.

Gazaix, A., et al. "Industrial Application of an Advanced Bi-level MDO Formulation to an Aircraft Engine Pylon Optimizationn." *AIAA Aviation Forum.* Dallas: American Institute of Aeronautics and Astronautics, Inc., 2019.

Gratz, Jennifer, John Jasa, and Jason Kirk. "Mission Analysis Demonstration for ONERA and University of Michigan." *Technical Exchange between NASA, ONERA, and University of Michigan.* Virtual: National Aeronautics and Space Administration, Scientific and Technical Information program, May 10, 2023.

Gray, Justin S., John T. Hwang, Joaquim R. R. A. Martins, Kenneth T. Moore, and Bret A. Naylor. "OpenMDAO: an open-source framework for multidisciplinary design, analysis, and optimization." *Structural and Multidisciplinary Optimization* 59, no. 4 (April 2019): 1075–1104.

Haimes, Robert, and John Dannenhoffer. "The Engineering Sketch Pad: A Solid-Modeling, Feature-Based, Web-Enabled System for Building Parametric Geometry." *21st AIAA Computational Fluid Dynamics Conference.* San Diego: American Institute of Aeronautics and Astronautics, Inc., 2013.

Hill, Geoffrey A., Osama A. Kandil, and Andrew S. Hahn. "Aerodynamic Investigations of an Advanced Over-the-Wing Nacelle Transport Aircraft Configuration." *Journal of Aircraft* 46, no. 1 (January 2009): 25–35.

Jones, D. R., M. Schonlau, and W. J. Welch. "Efficient Global Optimization of Expensive Black-Box Functions." *Journal Global Optimization* 13 (1998): 455–492.

Kelly, Matthew. "An Introduction to Trajectory Optimization: How to Do Your Own Direct Collocation." *SIAM Review* 59, no. 4 (2017): 849–904.

Kirby, Michelle R., and Dimitri N. Mavris. "The Environmental Design Space." *26th International Congress of the Aeronautical Sciences.* Anchorage: International Council of the Aeronautical Sciences, 2008.

Kulfan, Brenda M. "Universal Parametric Geometry Representation Method." *Journal of Aircraft* (American Institute of Aeronautics and Astronautics, Inc.) 45, no. 1 (2008): 141–158.

Lacy, Doug S., and Adam M. Clark. "Definition of Initial Landing and Takeoff Reference Configurations the High Lift Common Research Model (CRM-HL)." *AIAA AVIATION 2020 Forum.* Virtual: AIAA, 2020.

Lacy, Doug S., and Anthony J. Sclafani. "Development of the High Lift Common Research Model (HL-CRM): A Representative High Lift Configuration for Transonic Transports." *54th AIAA Aerospace Sciences Meeting.* San Diego: American Institute of Aeronautics and Astronautics, Inc, 2016.

Lambe, Andrew B., and Joaquim R. R. A. Martins. "Extensions to the Design Structure Matrix for the Description of Multidisciplinary Design, Analysis, and Optimization Processes." *Structural and Multidisciplinary Optimization* 46 (2012): 273–284.

Lee, Chung, and Dimitri Mavris. "Bayesian Collaborative Sampling for Aero-Propulsion Design of an Engine and Nacelle." *48th AIAA/ASME/SAE/ASEE Joint Propulsion Conference & Exhibit.* Atlanta: American Institute of Aeronautics and Astronautics, Inc., 2012.

Marfatia, Kiran J., and Jennifer D. Bergeson. *Aircraft Flaps Modeling in OpenMDAO.* White Paper, NASA Glenn Research

Center, Cleveland: National Aeronautics and Space Administration, Scientific and Technical Information Branch, 2021.

Martins, Joaquim R. R. A., and Andrew B. Lambe. "Multidisciplinary Design Optimization: a Survey of Architectures." *AIAA Journal* (American Institute of Aeronautics and Astronautics, Inc.) 51, no. 9 (2013): 2049–2075.

"Engine Selection: Parametric Cycle Analysis." In *Aircraft Engine Design*, by Jack D. Mattingly, William H. Heiser, & David T. Pratt, 95–137. Reston: American Institute of Aeronautics and Astronautics, 2002.

Mufti, Bilal, Mengzhen Chen, Christian Perron, and Dimitri N. Mavris. "A Multi-Fidelity Approximation of the Active Subspace Method for Surrogate Models with High-Dimensional Inputs." *AIAA AVIATION 2022 Forum.* Chicago and virtual, 2022.

Nunez, Luis Salas, Jimmy Tai, and Dimitri N. Mavris. "The Environmental Design Space: Modeling and Performance Updates." *AIAA SciTech 2021 Forum.* Virtual: American Institute of Aeronautics and Astronautics, Inc., 2021.

Rajaram, Dushhyanth, Raphael H. Gautier, Christian Perron, Olivia J. Pinon-Fischer, and Dimitri Mavris. "Non-Intrusive Parametric Reduced Order Models with High-Dimensional Inputs via Gradient-Free Active Subspace." *AIAA AVIATION 2020 FORUM.* Virtual: American Institute of Aeronautics and Astronautics, Inc., 2020.

Renganathan, Ashwin, et al. "Sensitivity Analysis of Aero-Propulsive Coupling for Over-Wing-Nacelle Concepts." *2018 AIAA Aerospace Sciences Meeting.* Kissimmee: American Institute of Aeronautics and Astronautics, Inc., 2018.

Tejero, Fernando, Matthew Robinson, David G. MacManus, and Christopher Sheaf. "Multi-objective Optimisation of Short Nacelles for High Bypass Ratio Engines." *Aerospace Science and Technology* (Elsevier Masson SAS) 91 (August 2019): 410–421.

The Dymos Development Team. *Aircraft Balanced Field Length Calculation.* NASA. 2022. https://openmdao.github.io/dymos/examples/balanced_field/balanced_field.html (accessed February 28, 2024).

—. *Modeling Dynamic Systems with Dymos.* 2022. https://openmdao.github.io/dymos/getting_started/intro_to_dymos/intro_ivp.html (accessed February 28, 2024).

The OpenMDAO Development Team. *Discrete Variables.* National Aeronautics and Space Administration. 2022. https://openmdao.org/newdocs/versions/latest/features/core_features/working_with_components/discrete_variables.html?highlight=discrete#discrete-variable-considerations (accessed February 29, 2024).

Tripathy, Rohit, Ilias Bilionis, and Marcial Gonzalez. "Gaussian Processes with Built-In Dimensionality Reduction: Applications to High-Dimensional Uncertainty Propagation." *Journal of Computational Physics* 321 (September 2016): 191–223.

United States Department of Transportation, Federal Aviation Administration. "Title 14 — Aeronautics and Space, Chapter I, Subchapter F, Part 91, Subpart B — Flight Rules." *eCFR.* Online. Washington, District of Columbia: United States Archives Records Administration, February 16, 2024.

Vassberg, J., M. Dehaan, M. Rivers, and R. Wahls. "Development of a Common Research Model for Applied CFD Validation Studies." *26th AIAA Applied Aerodynamics Conference.* Honolulu: American Institute of Aeronautics and Astronautics, Inc., 2008.

Wells, Douglas P., Bryce L. Horvath, and Linwood A. McCullers. *The Flight Optimization System Weights Estimation Method.* Technical Memorandum, NASA Langley Research Center, Hampton: National Aeronautics and Space Administration, Scientific and Technical Information program, 2017.

Zorumski, William E. *Aircraft Noise Prediction Program Theoretical Manual, Part 1.* Technical Memorandum, NASA Langley Research Center, Hampton: National Aeronautics and Space Administration, Scientific and Technical Information Branch, 1982.

Zorumski, William E. *Aircraft Noise Prediction Program Theoretical Manual, Part 2.* Technical Memorandum, NASA Langley Research Center, Hampton: National Aeronautics and Space Administration, Scientific and Technical Information Branch, 1982.